

Characterization of different high amylose starch granules. Part II: Structure evolution during digestion and distinct digestion mechanisms

Yu Tian^a, Bent Larsen Petersen^a, Xingxun Liu^b, Haiteng Li^c, Jacob Judas Kain Kirkensgaard^{d,e}, Kasper Enemark-Rasmussen^f, Bekzod Khakimov^d, Kim Henrik Hebelstrup^{g,h}, Yuyue Zhong^{a,**}, Andreas Blennow^{a,*}

^a Department of Plant and Environmental Sciences, University of Copenhagen, 1871, Frederiksberg C, Denmark

^b Lab of Food Soft Matter Structure and Advanced Manufacturing, College of Food Science and Engineering/Collaborative Innovation Center for Modern Grain Circulation and Safety/, Nanjing University of Finance and Economics, Nanjing, 210023, China

^c School of Food and Biological Engineering, Jiangsu University, Zhenjiang, 212013, China

^d Department of Food Science, University of Copenhagen, DK-1958, Frederiksberg C, Denmark

^e Niels Bohr Institute, University of Copenhagen, DK-2100, Copenhagen Ø, Denmark

^f Department of Chemistry, Technical University of Denmark, DK-2800, Kemitorvet, Building 207 Kgs. Lyngby, Denmark

^g Department of Agroecology, Section for Crop Genetics and Biotechnology, Aarhus University, 4200, Flakkebjerg, Denmark

^h PlantCarb ApS, Hørsholm, Denmark

ARTICLE INFO

Keywords:

High amylose
Resistant starch
Helical structure
Starch crystallinity
Lamellar structure
Digestibility

ABSTRACT

The objective of this research was to unravel the digestion of high amylose (AM) starch (HAS) granules through comparison of digestion of eight different types of HAS granules obtained from maize, potato, wheat, and barley. Unexpectedly, the resistant starch content (RS) of the HAS granules, ranging from 21% to 63%, did not correlate with the apparent AM content (AAC), which ranged from 34% to 97%. Instead, the pivotal factor governing digestibility was identified as the proportion of granules with smooth surfaces, in conjunction with the localized organization related to the arrangement of AM chains. Specifically, HAS granules originating from potato and maize, characterized by predominantly smooth-surfaced granules, as well as a higher double helix and B-type crystalline contents, exhibited higher RS content. Conversely, HAS granules sourced from wheat and barley, distinguished by a prevalence of granules with rough surfaces and high amorphous regions, displayed lower RS content. Furthermore, while potato and maize-derived HAS granules underwent minimal reorganization during digestion, those from wheat and barley underwent substantial molecular realignment. This phenomenon is likely attributed to the enhanced long AM molecules within wheat and barley, resulting in more significant degradation and molecular restructuring during digestion. The reorganized segments demonstrated increased resistance to enzymatic digestion. Thus, this study yields valuable insights into the mechanisms of the resistance of HAS granules to enzymatic digestion, emphasizing that AAC itself, within the range explored, does not emerge as a critical factor affecting their digestibility. The RS of HAS likely encompasses both pre-existing resistant structures and reorganized structures that form during digestion.

1. Introduction

Resistant starch (RS) is a key fraction of starch that evades digestion in the small intestine and reaches the colon where it is primarily fermented into short-chain fatty acids, thus conferring potential benefits to bowel health and disease prevention (A. Evans, 2016; Zhong, Qu, et al., 2022; Zhong, Tai, et al., 2022). Therefore, extensive research has aimed

at exploring and devising strategies to enhance RS fractions in food products. While starch in the human diet is often subjected to hydrothermal processing thereby losing its granular structure prior to ingestion, starch in low-moisture bakery foods like muesli and biscuits generally retains its granular structure (Roder et al., 2009; Roman, Sahagun, Gomez, & Martinez, 2019), especially for high amylose (AM) starches, which are known for their thermal stability. Additionally, raw,

* Corresponding author.

** Corresponding author.

E-mail addresses: yuyuezhong93@163.com (Y. Zhong), abl@plen.ku.dk (A. Blennow).

unprocessed starch is also incorporated in animal feeds (Weurding, Enting, & Versteegen, 2003), specific dairy products like acidified milk gels (R. Li et al., 2023) and foods including bananas and peanuts.

Notably, the apparent AM content (AAC) has been strongly positively correlated with RS levels from AAC of 0%–50% in various studies (Morita, Ito, Brown, Ando, & Kiriya, 2007; Song, Li, & Zhong, 2019b; Zhong, Tai, et al., 2022). High AM starch (HAS) granules (AAC \geq 50%) have been widely accepted as native, resistant starch sources (RS₂-enriched sources). The slow digestibility of HAS granules has been attributed to two main factors: (I) the absence of pores in HAS granules yields less effective attack sites (Tian, Wang, et al., 2023; Wang, Tian, Zhong, et al., 2023), and thus provides an effective barrier to enzyme access (Shrestha, Blazek, et al., 2012), and (II) the presence of B-type crystallites has been proposed to form larger “blocklets” (200–500 nm) than crystals in normal cereal starches (A-type crystallinity; 20–120 nm) at the periphery of starch granules, which is also associated with the absence of extensive pores and channels (H. Li, M. J. Gidley, & S. Dhital, 2019). Another mechanism that has been gradually accepted (Lopez-Rubio, Flanagan, Shrestha, Gidley, & Gilbert, 2008; Shrestha, Blazek, et al., 2012; Witt, Gidley, & Gilbert, 2010) involves cleaved starch molecules that reorganize during digestion and form more resistant segments. However, due to the lack of sufficient HAS varieties in decades, such conclusions or hypotheses were generally drawn from starches with a wide range of AAC of same crops, typically around 0–70%. This raises the question: Is AAC still the most important factor affecting the digestibility of various HAS granules which all exhibit relative high AM content, e.g., AAC ranging from 30% to 100%?

Numerous efforts have been made to breed and genetically engineer high AAC varieties from different botanical sources. Two strategies have been employed to increase AAC: suppression of DBE (debranching enzymes) or SS (starch synthases) expression to suppress the synthesis of amylopectin within the amyloplast, or downregulation of SBE (starch branching enzymes) to generate “AM-like” materials (Haiteng Li, Michael J Gidley, & Sushil Dhital, 2019; Zhong, Tai, et al., 2022). To date, various HAS granules and varieties with AM-only genotypes have been successfully generated from wheat (Regina et al., 2006), barley (Carciofi et al., 2012), potato (Blennow et al., 2005), rice (Kong, Zhu, Sui, & Bao, 2015), and maize (Zhang et al., 2018; Zhong, Wu, et al., 2020). However, recent studies (H. Li et al., 2020a; Haiteng Li et al., 2022; R. Li et al., 2023) that compared HAS granules from different botanical sources have shown that the observed differences in functionality cannot be solely explained by AAC. Moreover, even within starches with similar AAC originating from the same botanical source, variations in digestibility are observed, due to the differences in the fine molecular structural features of amylose (Syahariza, Sar, Hasjim, Tiz-zotti, & Gilbert, 2013).

Moreover, our recent investigations (Tian, Liu, et al., 2023) have revealed that different HAS granules exhibit diverse multi-scale structures and varying thermal stability, even when having similar AAC, which is related to the content of double helices. Based on these findings, we hypothesized that AAC is not the most important factor affecting the digestibility of HAS granules. Thus, to further explore the digestibility of HAS granules, we collected eight types of HAS granules from different botanical sources (details in section 2.1), analyzed their multi-scale structural changes before and after *in vitro* digestion, and discussed possible underlying mechanisms for digestive resistance. This study provides valuable insight into the degree of enzymatic digestion of HAS.

2. Materials and methods

2.1. Starch and enzyme sources

Eight different HAS was collected, including five types of maize HAS granules (NAFU50 and NAFU60 from China (Song, Li, & Zhong, 2019a; Zhong, Qu, Blennow, Liu, & Guo, 2021), HylonVII from USA (L. Li, Jiang, Campbell, Blanco, & Jane, 2008), and Gelose 50 and Gelose 80

from Australia (Penford Australia Ltd.), one HAS from potato (Blennow et al., 2005), one HAS from wheat (HAW5) (unknown genetic background, a gift from Northwest A&F University), and one AM-only barley starch (AOBS) (Carciofi et al., 2012). AAC was reported previously (Fig. 1) (Tian, Liu, et al., 2023). Pancreatin (A7545) and Amyloglucosidase (A7095) were purchased from Sigma-Aldrich (USA); Isoamylase (E-ISAMY, 200 U/mL) was purchased from Megazyme (Ireland). Other chemical reagents were from Sigma-Aldrich (USA).

2.2. *In vitro* digestion and resistant starch content

In vitro digestion was performed in accordance to the method of Tian (Tian, Wang, et al., 2023) with minor modification. Twenty mg of starch powder was dispersed in 1 mL of 50 mM sodium acetate buffer (containing 5 mM calcium chloride, pH 5.5) and was incubated at 37 °C for 5 min while being stirred at 900 rpm. Then 1 mL of enzyme solution containing 4.8 mg pancreatin and 4.3 μ L amyloglucosidase in sodium acetate buffer (pH 5.5) was added with moderate magnetic stirring. 0.05 mL aliquots were then mixed with 0.5 mL absolute ethanol at 0, 5, 10, 20, 40, 60, 120, 160, and 180 min and the glucose concentration determined by the D-glucose (GOPOD Format) assay. The digestibility curves were analyzed using the log of slope (LOS) application to 1st order kinetics (C. H. Edwards, Warren, Milligan, Butterworth, & Ellis, 2014) to obtain values for the digestibility rate constants, k_1 and k_2 . It is worth noting that the LOS method is optimal for identifying complex first-order kinetic processes and their respective regions within the data, which we aim at here. However, it relies on the numerical differentiation of discrete rate data points, which may introduce inherent inaccuracies. Alternatively, a more precise analysis, albeit not generating first-order kinetic interpretations, could be achieved for future analysis by utilizing a non-linear least-squares fitting (NLLS) method as suggested (Yu et al., 2018).

RS fractions were prepared after prolonged hydrolysis time, referring to the *in vivo* transit time of 10 h (Edwards et al., 2015; Worsøe et al., 2011), and collected as described above. The reaction was stopped by adding 0.3 M Na₂CO₃ (final concentration) and centrifuged at 3000 g, 10 min at RT, to separate the remaining residues, which was considered as RS and the RS was washed with MilliQ water three times and freeze dried. The dry residues were weighed and the RS content (% of the original starch weight) were calculated.

2.3. Amylopectin and AM chain length distribution (CLD) determined by high performance anion exchange chromatography with pulsed amperometric detection (HPAEC-PAD)

Starch samples (5 mg, dry basis) were prepared in a 0.01 M sodium acetate buffer (5 mg/mL, pH 4.0) and subjected to gelatinization at 130 °C for 1 h. Following this, the gelatinized samples underwent debranching by adding 2 μ L isoamylase (0.4 U) and incubating at 40 °C for 3 h. Subsequently, 40 μ L of the debranched samples (5 mg/mL) were separated on a CarboPac PA-200 column, integrated with an HPAEC-PAD system from Dionex (Sunnyvale, CA, USA). Peak integration and corrections for detector response to account for mass bias (Wong & Jane, 1995) were conducted as previously described (Blennow, Bay-Smith, Wischmann, Olsen, & Møller, 1998).

2.4. Molecular size distribution (SEC)

The size distributions of whole starch molecules and starch chains obtained after enzymatic debranching were analyzed as described (Hongyan Li, Prakash, Nicholson, Fitzgerald, & Gilbert, 2016) with minor modifications, using the size exclusion chromatography-triple detector array SEC-TDA (Viscotek, Malvern, UK) equipped with GRAM 1000 SEC columns (Polymer Standards Service GmbH, Mainz, Germany) connected to a refractive index detector (PN3140, PostNova Analytics, Landsberg, Germany). For the whole starch, samples (5 mg) were

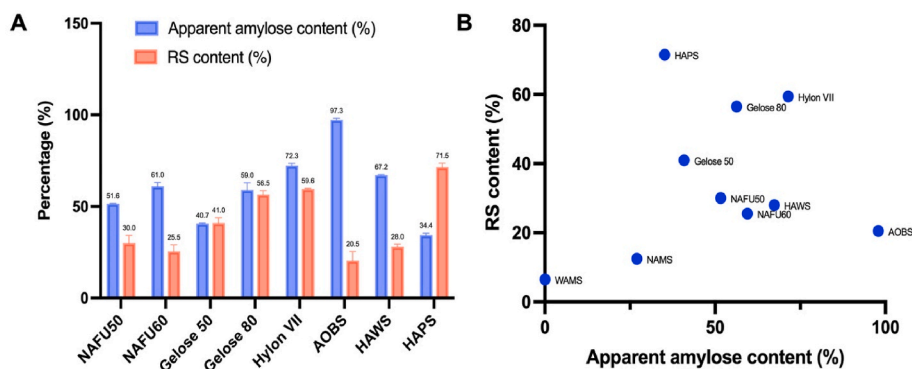


Fig. 1. Apparent amylose content (AAC) and resistant starch (RS) content of eight different starches.

dissolved in 1 mL DMSO/LiBr (0.5% w/w, Avantor, US) at 80 °C overnight and centrifuged at 20,000 g for 5 min, and the supernatant was injected in the SEC system. Elution was performed using DMSO/LiBr at a flow rate of 0.5 mL/min and a column temperature of 65 °C. Debranched samples were prepared by heating starch dispersion in screwed tubes with DMSO/LiBr (5 mg/ml) at 80 °C for 3h, the gelatinized starch was collected after centrifugation at 4000g for 10 min with absolute ethanol and allowed to dry in a fume hood at ambient temperature. Debranched samples were prepared by adding 2 μ L isoamylase (0.4 U) in 1 mL sodium acetate buffer (0.01M, pH 4.0) which were incubated at 40 °C for 3 h and freeze dried. 5 mg/ml debranched samples dissolved in DMSO/LiBr were prepared before injecting onto the SEC system.

The distribution of AM chain lengths (CLD) was fitted to an AM biosynthesis model (Fig. S1) (Nada, Zou, Li, & Gilbert, 2017). The length of chains, and the amount of chains in each fitting region, are represented by the parameters of β_{AmX} and h_{AmX} ($X = 1-3$); e.g. the higher the β_{AmX} value, the shorter the chain, and the higher the h_{AmX} value, the higher the amount of chains in the region X (region 1 is low degree of polymerization (DP) region of AM, region 2 is intermediate DP region of AM and region 3 is high DP region of AM).

2.5. Proton nuclear magnetic resonance (1H NMR) spectroscopy

A 600 MHz NMR spectrometer (Bruker Avance III, Bruker Biospin, Rheinstetten, Germany) was used to obtain one-dimensional 1H NMR spectra of starch samples. The details of sample preparation and NMR spectrum acquisition are similar as described (Tian, Liu, et al., 2023). Using areas of signals representing anomeric protons (δ 5.35–5.45 α -1,4 and δ 4.95–5.00 α -1,6) to calculate the degree of glucan branching of starch. The Sigma software (Khakimov, Mobaraki, Trimigno, Aru, & Engelsen, 2020) was used to detect and calculate the signal areas.

2.6. Solid-state ^{13}C nuclear magnetic resonance (^{13}C NMR)

The solid-state ^{13}C NMR analysis of starch was performed on a Bruker AV-300 spectrometer as described (Tan, Flanagan, Halley, Whittaker, & Gidley, 2007). Amorphous standard samples were prepared from starch suspension (1% w/v, in MilliQ water of waxy maize, waxy wheat, waxy barley, and waxy potato) was heated at 99 °C for 30 min, snap frozen in liq N_2 and freeze dried. Approximately 300 mg starch was packed in a 4-mm diameter rotor and the rotor was spun at 5–6 kHz at the magic angle (54.7°). The 90° pulse width was 5 μ s and a contact time of 1 ms was used for all starch samples with a recycle delay of 5 s. At least 2400 scans were accumulated for each spectrum with spectral width of 38 kHz, with an acquisition time of 3 ms. The relative content of single helices (102–103 ppm), double helices (99–101 ppm) and the amorphous region were calculated as described (Tan et al., 2007).

2.7. Small-angle X-ray scattering (SAXS)

The starch nano-lamellar structure was analyzed on a Nano-inXider instrument (Xenocs SAS, Grenoble, France). Starch powder was dissolved with excess MilliQ water and placed at 4 °C overnight. The suspension was centrifuged at 5000 g for 5 min, the supernatant was removed, and the remaining suspension (0.7 mL) was placed in 1-mm-thick sample cells for further measurement. The fitting of the data including the thickness of crystalline (dc) and amorphous (da) lamellae was carried out using the approach described before (Kuang et al., 2017).

$$\gamma I(r) = \int_0^\infty I(q) q^2 \cos(qr) dq / Q$$

$$Q = \int_0^\infty I(q) q^2 dq$$

where $I(q)$ is the scattering intensity, q is the scattering vector defined as $q = 4\pi \sin\theta / \lambda$ (2θ is the scattering angle) and r is the direction along the lamellar stack.

2.8. Wide angle X-ray scattering (WAXS)

After conditioning the sample with saturated KCl for 72 h in a humidity chamber with a relative humidity of 90%, a Nano-inXider instrument (Xenocs SAS, Grenoble, France) was used to analyze the samples using 40 mA current, 40 kV voltage and 0.1542 nm wavelength Cu $K\alpha$ radiation. The radial average intensity I is given as a function of the scattering angle 2θ in the range of 5–40°. The calculation of relative crystallinity was using a PeakFit software (version 4.12 Systat Software, Inc., San Jose, CA, USA) to estimate the amorphous background scattering and calculate the relative crystallinity as follow (Tian et al., 2021):

$$\text{Relative crystallinity (\%)} = \text{Peak areas} / \text{Total area}$$

2.9. Fourier transform infrared - attenuated total reflectance (FTIR-ATR) spectroscopy

FTIR-ATR spectroscopy was performed using a Bomem MB100 FTIR spectrometer equipped with a Golden gate attenuated total reflectance (ATR) accessory. The starch samples were first equilibrated to match the ambient laboratory humidity. Spectra were collected at a resolution of 4 cm^{-1} and co-added for each sample. Background spectra were obtained by cleaning the crystal with a mixture of ethanol and water and recording 128 co-added scans. Lorentzian line shape with a half-width of 19 cm^{-1} and a resolution enhancement factor of 1.9 was assumed. After baseline correction and deconvolution analysis using OMNIC software,

IR absorbance values at 1022 and 1045 cm^{-1} were extracted from the spectra (Tian, Wang, et al., 2023).

2.10. Morphological observation

The detailed topography and morphology of the starch granules were monitored by Field Emission Scanning Electron Microscopy (FE-SEM) (FEI Quanta 200) after fixing and sputter-coating granules with gold (Wang, Tian, Christensen, et al., 2023).

2.11. Statistical analysis

All experiments were carried out in triplicate, and data were presented as average value \pm standard error. Determination of significant difference between average values and Pearson's correlation analysis were done in SPSS 20.0 (SPSS Inc., Chicago, IL), followed by Duncan's post hoc test at 95% confidence level ($p < 0.05$).

3. Results

3.1. Digestibility and RS content

The AAC of HAS granules within the 35–100% AAC window and the corresponding RS content (Fig. 1A) and their scattering plot (Fig. 1B) showed that AAC and RS were not positively correlated. HAS from potato (HAPS), which has the lowest AAC (34.4%), displayed the highest RS content (62%) compared to other HAS granules with higher AAC. In contrast, AOBs, which has the highest AAC (97%), had a relatively lower RS content (21%). Among the five HAS granules from maize (HAMs) (NAFU50, NAFU60, Gelose 50, Gelose 80, and Hylon VII), although Hylon VII demonstrated the highest RS content consistent with its high

AAC, no positive correlation between AAC and RS content was found in the other four HAS granules from maize. Thus, the resistance to enzyme digestion increases markedly with AAC from low AM starch to high AM starch (Haiteng Li, Michael J. Gidley, & Sushil Dhital, 2019; Liu et al., 2020; Zhong, Tai, et al., 2022) does not hold for a window that only have HAS granules.

The digestion profiles of different HAS granules (Fig. 2A) showed that HAMs and HAPS digested slowly throughout the entire digestion process, while AOBs and HAS from wheat (HAWs) were digested much faster during the initial 40 min, followed by a slower digestion phase. The LOS fitting depicted in Fig. 2B, as described by (Edwards et al., 2014), demonstrated that HAS granules followed first-order digestion kinetics and exhibited a two-phase digestion pattern: an initial fast digestion step (Phase I) followed by a slower second step (Phase II). However, our study indicates that the two-phase digestion is unlikely to be solely due to substrate accessibility in a complex food system, such as protection by protein and fiber matrices in e.g. pasta made from durum wheat (Edwards et al., 2014). The AOBs demonstrated prominent inflection points and discontinuity, which is hypothesized to be due to the presence of different species at different times of digestion, as suggested (Evans & Thompson, 2008). The values of k_1 and k_2 obtained from the fit presented in Table 1 revealed that in the first phase (digestion time 0–80 min), the starches NAFU50, NAFU60, Gelose 50, Gelose 80, HAWs, and AOBs had much higher degradation rate coefficients than in the second step (80–180 min), with AOBs showing the most significant decrease in digestion rate. The LOS plots of HAPS and Hylon VII displayed almost continuous linearities (Fig. 1B).

However, the digestion profiles of HAS granules mainly showed that AOBs and HAWs, i.e., HAS granules from wheat and barley, exhibited the highest digestibility (rate and percentage) and the lowest enzymatic resistance throughout the entire digestion process, even with their

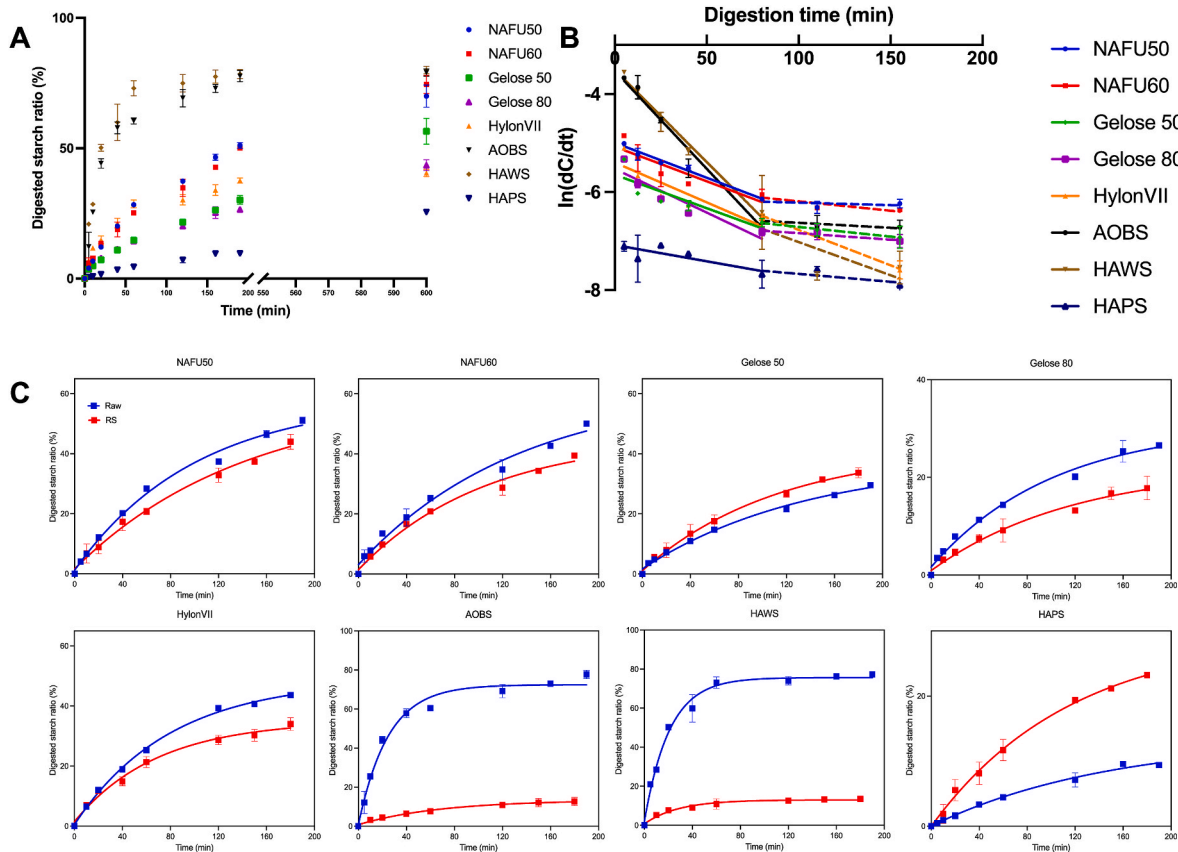


Fig. 2. *In vitro* digestion of eight raw starches (A) and typical Logarithm of Slope (LOS) plots obtained from digestibility data (B), and starch digestibility compare of raw starch and resistant starch (RS) (C).

Table 1
RS content and parameters of native starch digestibility estimated from the LOS.

Samples	RS (%)	C180-difference (%)	k_1 (min ⁻¹)	k_2 (min ⁻¹)
NAFU50	30.0 ± 3.0 ^d	(-)7.1 ± 2.5 ^c	-0.014 ± 0.000 ^a	-0.001 ± 0.000 ^a
NAFU60	25.5 ± 2.5 ^{de}	(-)10.6 ± 0. ^c	-0.015 ± 0.003 ^a	-0.003 ± 0.001 ^a
Gelose 50	41.0 ± 3.3 ^c	(+)4.1 ± 1.7 ^b	-0.014 ± 0.001 ^a	-0.004 ± 0.002 ^a
Gelose 80	56.5 ± 1.7 ^b	(-)5.8 ± 1.8 ^c	-0.018 ± 0.000 ^a	-0.003 ± 0.001 ^a
HylonVII	59.6 ± 0.5 ^a	(-)5.6 ± 1.5 ^b	-0.011 ± 0.001 ^a	-0.011 ± 0.000 ^a
AOBS	20.5 ± 3.5 ^e	(-)65.0 ± 0.0 ^d	-0.040 ± 0.001 ^b	-0.002 ± 0.001 ^a
HAWS	28.0 ± 1.0 ^d	(-)63.8 ± 0.6 ^d	-0.038 ± 0.001 ^b	-0.010 ± 0.002 ^a
HAPS	71.5 ± 1.5 ^a	(+)14.4 ± 0.8 ^a	-0.005 ± 0.000 ^a	-0.005 ± 0.000 ^a

k_1 , the digestion rate of starch in the first stage (0–80 min); k_2 , the digestion rate of starch in the second stage (80–180 min); Resistant starch (RS), the residuals percentage of starch digestion endpoint at 10h; C_{180-difference}: difference of digested ratio at 180 min of raw starch and resistant starch (C_{180-RS}-C_{180-raw} %). The raw data for all samples is listed in Table S1. Values are means ± standard deviation. Values with different letters in the same column are significantly different at $p < 0.05$, $n = 2$.

relatively high AAC values of 97% and 67%, respectively. In comparison, HAS from potato (HAPS) and HAS from maize (Gelose 50), with much lower AAC values of 34% and 40%, respectively, than AOBS and HAWS, showed higher enzymatic resistance. These findings confirm that

the digestibility of HAS is not solely related to AAC, but rather associated with unique starch structures, which is partly influenced by the botanical source, and also additional factors such as crop growth conditions.

The comparison of enzymatic resistance between HAS granules and their RS residues, as depicted in Fig. 2C, revealed that the enzymatic resistance of HAS granules can either be enhanced or weakened during the digestion process. Specifically, 1) AOBS and HAWS exhibited lower digestograms in which the RS starch displayed significantly lower digestion levels compared to their respective native starches, indicating an enhanced level of enzymatic resistance. 2) The digestograms for HAMs demonstrated relatively unchanged curves, with a slight increase in digestion levels observed for Gelose 50, while other varieties (NAFU50, NAFU60, Gelose 80, and Hylon VII) exhibited decreased digestion. The discrepancies in digestion levels between the native starches and their digestion residues (RS) were relatively minimal for HAMs. 3) HAPS showcased an opposing trend, revealing decreased enzymatic resistance for RS compared to raw starch (the undigested starch). These findings confirm the existence of distinct response mechanisms within the digestion process of HAS, as discussed in section 4.1.

3.2. Molecular size distribution and chain length distribution (CLD) by SEC

The molecular size distribution of the native (not debranched) samples, as analyzed by size exclusion chromatography (SEC), revealed two main components referred to as AP and AM fractions (Fig. 3A and Fig. S1). From raw starch to their RS residues, both AP and AM molecules in all HAS granules showed a decrease in hydrodynamic radius (R_h) due to digestive enzyme-induced molecular hydrolysis, with the

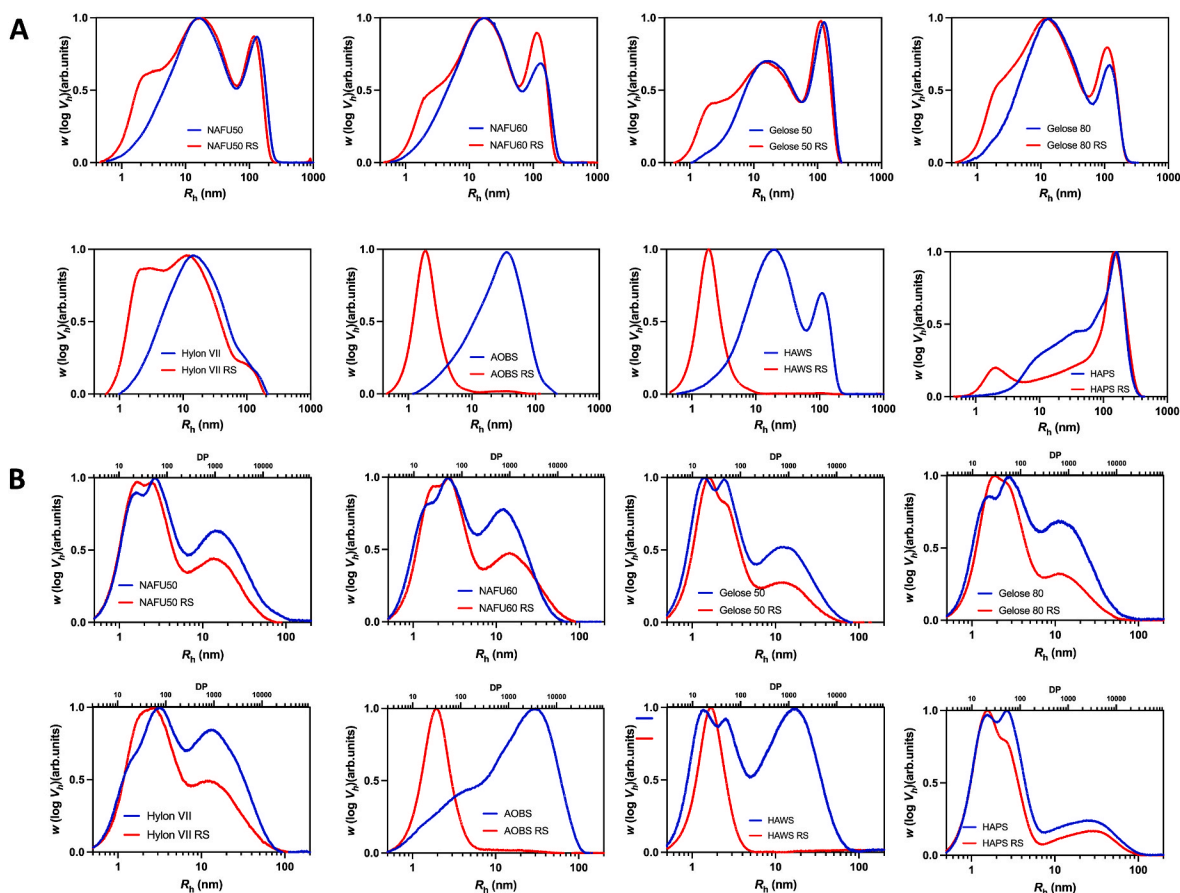


Fig. 3. Size exclusion chromatography (SEC) weight distributions of whole (fully branched) starch molecules (A) and chain length distribution (CLD) obtained by SEC analysis of debranched starch molecules (B) of raw starch and resistant starch (RS).

most significant changes observed for AOBS and HAWS (Table 2).

As a result of *in vitro* digestion of different HAS granules, the area under the curve of AM fractions (Rh < 100 nm) became substantial for most samples. This observation may be attributed to cleaved AP molecules having a similar Rh to AM molecules, co-eluting with AM molecules and detected by the RI monitor of SEC. The most significant molecular degradation was found in AOBS and HAWS, aligning with their highest enzymatic susceptibility observed in Fig. 2A. The appearance of molecules with Rh 1–4 nm (with a peak maximum at ~ Rh 2 nm) in each RS sample is consistent with the presence of enzyme-resistant dextrans observed after prolonged *in vitro* digestion of extruded starches (Witt et al., 2010), as well as native maize starch and potato granules (Teng, Witt, Wang, Li, & Hasjim, 2016). Apparently, AM-rich starches, especially AOBS and HAWS, had high amounts of such enzyme-resistant dextrans after digestion, while HAPS with the lowest AAC showed the lowest amounts of these dextrans (Fig. 3A). This suggests that cleaved AM molecules might be the main contributor to the formation of enzyme-resistant dextrans.

The CLD profiles of debranched samples (Fig. 3B) exhibited three main, but overlapping, components: short amylopectin (AP₁, degree of polymerization (DP) 6–36), long amylopectin (AP₂, DP 37–100), and AM chains (AM, DP > 100), as previously reported (Zhong, Liu, et al., 2020). The AM content (AC) extracted from SEC data of debranched starches (Table S2, RC_{de-AM}) was consistent with the AAC data; that is, the AC of AOBS was the highest, followed by HylonVII and HAWS. The area under the curve in the AM region decreased significantly in all RS residues, while the AP region was less affected, suggesting greater enzymatic susceptibility of AM molecules compared to AP molecules, in agreement with the hypothesis above. Long AP chains were also partly degraded, especially for the starches with shorter AP₂, such as Gelose 50 and HAPS.

In RS residues of HAS granules from maize and HAPS, three main

components were still found, indicating that their structures were not severely disrupted by enzymes. However, RS residues of AOBS and HAWS showed only one component with DP 10–40 (Rh 1–5 nm), which highly overlapped with their profiles before debranching (Fig. S1D), indicating they were predominantly dextrans with very short and few branches (α -1,6 links still exist in the RS, as indicated in Table S4).

Overall, the SEC data displayed two types of digestion degradation patterns of HAS granules at the molecular level: (I) AM and AP molecules (HAWS and AOBS) were remarkably degraded into small chains with DP 10–40, forming highly enzymatically re-organized structures; (II) AM and long AP molecules were partially degraded, but all molecules still remained (HAMSS and HAPS).

3.3. Amylopectin chain length distribution (CLD) by HPAEC-PAD

The changes in the CLD of the AP molecules in HAS granules upon digestion (Fig. 4A and B) mainly showed degradation of AP side chains with DP 12–24 and DP > 42. AP chains with DP > 42 can be regarded as the backbone chains in the AP structure, perpendicularly connecting all shorter side chains, and the chains with DP 12–24 act as connector chains between the double helix and backbone chains, both of which are located in the amorphous lamellae (Zhong, Bertoft, Li, Blennow, & Liu, 2020). Hence, their degradation upon digestion suggests that enzymes mainly targeted the amorphous lamellae in the crystalline region, in addition to the amorphous region.

Notably, the amounts of AP chains with DP 25–42 in HAS granules increased after digestion, and we suggest that this increase is due to the degradation of backbone chains. The backbone chains are initially cleaved into small segments, but the presence of branching points in the backbone chains prevents α -amylase and amyloglucosidase from further hydrolyzing the chains, causing the enzymes to diffuse away.

It is noteworthy that NAFU50 and NAFU60 exhibited fewer changes

Table 2

The changes of average chain lengths (ACL) of debranched AP and AM fractions of RS samples compared with native corresponding.

Sample	RC _{de-AP1} (%)	RC _{de-AP2} (%)	RC _{de-AM} (%)	ACL _{de-AP1}	ACL _{de-AP2}	ACL _{de-AM}	β_{Am1} × 10 ⁻³	h_{Am1} × 10 ⁻¹	β_{Am2} × 10 ⁻³	h_{Am2} × 10 ⁻¹	β_{Am3} × 10 ⁻⁴	h_{Am3} × 10 ⁻¹	Rh _{na-AP} (nm)	Rh _{na-AM} (nm)	RC _{na-AP} (%)	RC _{na-AM} (%)
NAFU50	(+) 5.6 ± 0.2 ^{de}	(+) 4.6 ± 0.2 ^d	(-) 10.2 ± 0.4 ^{bc}	(+) 0.6 ± 0.0 ^{cd}	(-) 3.9 ± 0.2 ^{ab}	(-) 35.6 ± 1.0 ^c	(-) 0.2 ± 0.5 ^{cd}	(-) 0.5 ± 0.1 ^{ab}	(-) 0.0 ± 0.1 ^{bc}	(-) 1.1 ± 0.1 ^b	(+) 1.0 ± 0.1 ^b	(-) 1.2 ± 0.1 ^{bc}	(-) 13.4 ± 1.1 ^d	(-) 3.1 ± 0.0 ^{ab}	(-) 3.9 ± 0.3 ^c	(+) 3.9 ± 0.3 ^c
NAFU60	(+) 4.1 ± 1.1 ^e	(+) 4.2 ± 0.5 ^d	(-) 8.3 ± 0.6 ^b	(+) 0.7 ± 0.2 ^{cd}	(-) 4.6 ± 0.8 ^{ab}	(+) 240.8 ± 26.2 ^a	(-) 0.4 ± 0.5 ^{cd}	(-) 0.8 ± 0.2 ^{ab}	(-) 0.4 ± 0.3 ^{cd}	(-) 1.6 ± 0.0 ^{bc}	(-) 1.9 ± 1.2 ^d	(-) 0.5 ± 0.4 ^a	(-) 7.0 ± 2.1 ^{cd}	(-) 2.3 ± 0.1 ^a	(+) 2.3 ± 0.4 ^b	(-) 2.3 ± 0.4 ^d
Gelose50	(+) 6.4 ± 1.4 ^{cde}	(+) 4.4 ± 0.9 ^d	(-) 10.8 ± 0.5 ^c	(+) 0.9 ± 0.7 ^{cd}	(-) 3.4 ± 0.6 ^a	(+) 19.6 ± 17.0 ^b	(+) 1.3 ± 0.3 ^{bc}	(-) 1.1 ± 0.2 ^b	(+) 0.4 ± 0.1 ^b	(-) 1.3 ± 0.2 ^{bc}	(+) 0.9 ± 0.2 ^b	(-) 0.7 ± 0.0 ^{ab}	(-) 8.0 ± 0.3 ^{cd}	(-) 4.0 ± 0.1 ^b	(-) 3.3 ± 0.1 ^c	(+) 3.3 ± 0.1 ^c
Gelose80	(+) 8.2 ± 0.4 ^{cd}	(+) 7.7 ± 0.3 ^c	(-) 15.9 ± 0.1 ^d	(+) 0.8 ± 0.2 ^{cd}	(-) 7.4 ± 4.3 ^b	(+) 40.4 ± 4.3 ^b	(+) 2.3 ± 0.3 ^b	(-) 2.3 ± 0.2 ^c	(+) 0.5 ± 0.1 ^b	(-) 3.0 ± 0.1 ^d	(+) 1.1 ± 0.2 ^{cd}	(-) 1.5 ± 0.1 ^{cd}	(-) 6.4 ± 0.6 ^{cd}	(-) 3.1 ± 0.5 ^{ab}	(+) 2.6 ± 1.8 ^b	(-) 2.6 ± 1.8 ^d
Hylon VII	(+) 8.0 ± 1.3 ^{cd}	(+) 8.3 ± 0.2 ^c	(-) 16.4 ± 1.1 ^d	(+) 0.1 ± 0.0 ^{cd}	(-) 6.4 ± 1.0 ^{bc}	(-) 6.1 ± 11.2 ^{bc}	(+) 1.1 ± 0.4 ^{bc}	(-) 0.8 ± 0.2 ^{ab}	(+) 0.1 ± 0.1 ^{bc}	(-) 1.9 ± 0.4 ^c	(+) 0.0 ± 0.0 ^{bc}	(-) 1.9 ± 0.2 ^d	(-) 0.9 ± 5.1 ^c	(-) 3.8 ± 0.0 ^b	(-) 1.6 ± 0.8 ^c	(+) 1.6 ± 0.8 ^c
AOBS	(+) 43.7 ± 0.7 ^a	(+) 27.5 ± 0.1 ^a	(-) 71.2 ± 0.7 ^f	(+) 2.0 ± 1.1 ^{ac}	(-) 35.2 ± 1.7 ^e	(-) 654.7 ± 12.0 ^d	(-) 12.9 ± 0.4 ^a	(-) 2.4 ± 0.0 ^c	(-) 2.1 ± 0.1 ^a	(+) 5.5 ± 0.2 ^e	(-) 4.8 ± 0.3 ^a	(-) 5.3 ± 0.1 ^e	ND	(-) 9.6 ± 0.2 ^d	(-) 11.0 ± 0.5 ^d	(+) 11.0 ± 0.5 ^b
HAWS	(+) 37.3 ± 0.5 ^b	(+) 12.5 ± 0.1 ^b	(-) 48.5 ± 0.7 ^e	(+) 3.4 ± 0.5 ^a	(-) 22.6 ± 0.0 ^d	ND	ND	ND	ND	ND	ND	ND	ND	(-) 7.9 ± 0.1 ^c	(-) 20.2 ± 0.5 ^e	(+) 20.2 ± 0.5 ^a
HAPS	(+) 8.9 ± 0.3 ^c	(-) 3.8 ± 0.1 ^c	(-) 5.1 ± 0.4 ^a	(-) 0.4 ± 0.1 ^d	(-) 4.9 ± 0.0 ^{abc}	(+) 273.9 ± 15.5 ^a	(-) 2.4 ± 1.5 ^d	(-) 0.2 ± 0.1 ^a	(-) 0.6 ± 0.1 ^d	(-) 0.4 ± 0.0 ^a	(-) 0.8 ± 0.1 ^{cd}	(-) 0.6 ± 0.0 ^{ab}	(+) 14.6 ± 3.3 ^b	(-) 10.4 ± 0.5 ^d	(+) 11.9 ± 0.8 ^a	(-) 11.9 ± 0.8 ^e

The differentiation values are calculated by the parameters of RS samples minus raw samples, (+) denotes an increase during digestion and (-) denotes a decrease. The actual values of each sample are listed in Table S2. Values are means ± standard deviation. Values with different letters in the same column are significantly different at p < 0.05, n = 2.

RC_{de-X}: relative amount of fraction X of debranched sample; RC_{na-X}: relative amount of fraction X of native sample; ACL_{de-X}: the average chain length (DP) of the fraction X of debranched sample; Rh_{na-X}: hydrodynamic radius of fraction X of native sample. β_{Ami} : higher value means shorter chains in the ith region; h_{Ami} : higher value means higher amount of chains in the ith region. Region 1: low DP region of amylose. Region 2: intermediate DP region of amylose. Region 3: high DP region of amylose. ND: not detected.

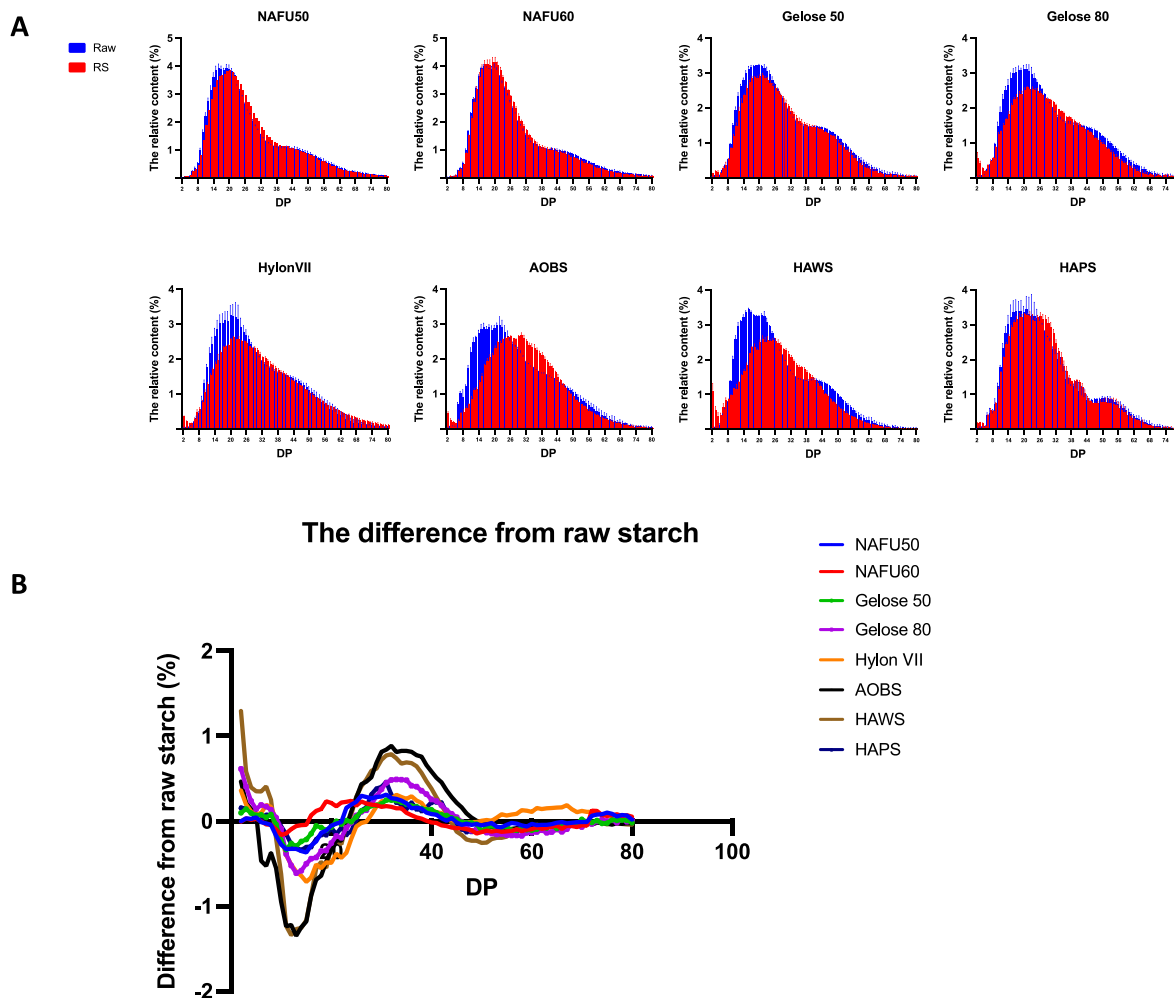


Fig. 4. Chain length distribution (CLD) profiles of raw starch (blue) and resistant starch (RS) (red) debranched starch characterized by high performance anion exchange chromatography with pulsed amperometric detection (HPAEC-PAD) (A); amylopectin chain length distribution difference between RS and corresponding raw starches (B).

in AP CLD compared to the other HAMSs. This observation may be explained by a higher presence of AM molecules oriented in the amorphous lamellae, which may act as a barrier to enzyme access (Zhong, Liu, et al., 2020). For AOBS and HAWS, a significant decrease in the relative content (RC) of fa (DP 6–12) was observed. This decrease can possibly be attributed to two factors: (I) AOBS and HAWS being enriched in single helical structure (data in section 3.5), which is more enzymatically susceptible than a double helical structure (Man et al., 2013), and (II) they exhibited more crystalline defects and less crystallized regions (data in section 3.6).

However, the impact of longer amylopectin chains (DP > 80) on the digestibility of HAS remains uncertain in this study. This uncertainty arises from the limitations of quantitatively detecting chains above DP \approx 70 using HPAEC and the challenges associated with band broadening in SEC, which might potentially be addressed by applying the developed model to differentiate the fine structural features of these longer amylopectin chains (Yu et al., 2019).

3.4. Degree of branching

The degree of branching, as deduced from the α -1,6 linkage: α -1,4 linkage ratios of the HAS granules and their RS residues, as quantified from the ^1H NMR spectra (Fig. S3 and Table S4) (Table 4), revealed that the hydrolytic enzymes preferred to attack α -1,4 linkages in the samples.

As a result, most RS residues showed an increase in the relative ratio of α -1,6 to α -1,4 linkages, except for those of AOBS and HAPS. Porcine pancreatic α -amylase is an endo-acting enzyme that primarily cleaves α -1,4 linkages to generate maltose and soluble oligosaccharides, including maltotriose, maltotetraose, and α -limit dextrins (Ishikawa, Matsui, Honda, & Nakatani, 1990). On the other hand, AMG is exo-acting and hydrolyzes both α -1,4 and α -1,6 linkages, with a specific activity on α -1,6 linkages only 0.2% that on α -1,4 linkages (Norouziyan, Akbarzadeh, Scharer, & Moo Young, 2006). Therefore, during digestion, the hydrolysis of α -1,4 linkages is more prominent than that of α -1,6 linkages, resulting in an increased ratio of α -1,6 to α -1,4 linkages (see Table 5).

Among the HAS granules (except for HAPS), NAFU50, NAFU60, and HAWS exhibited a higher increase in the α -1,6 to α -1,4 linkages ratio compared to Gelose 50, Gelose 80, and Hylon VII. This observation is consistent with the RS content results (Table 1), indicating that a greater proportion of α -1,4 linkages in NAFU50, NAFU60, and HAWS were hydrolyzed, likely due to the relatively higher amount of non-double helix state short branch chains (fa) (Tables S3 and S4).

The consistent α -1,6 to α -1,4 linkage ratios observed in AOBS and HAPS, when compared with the corresponding RS, may stem from different factors. In AOBS, the presence of a few branches and its “AM-like” structure, characterized by short branches (short fa) and ample space between branches (Table S3), primarily contribute to this

Table 3

The changes of amylopectin molecular sub-chain structures of RS samples compared with native corresponding.

Samples	Average chain lengths (ACLs) (DP)				Relative proportions (RC) (%)			
	fa	fb ₁	fb ₂	fb ₃	fa	fb ₁	fb ₂	fb ₃
NAFU50	(+)	(+)	(+)	(-)	(-)	(-)	(+)	(-)
	0.2	0.4	0.1 ±	1.1	1.3	2.5 ±	2.8	0.5 ±
	±	±	0.0 ^{bc}	±	±	0.4 ^{ab}	±	0.3 ^{abc}
	0.0 ^b	0.2 ^a		0.4 ^a	0.4 ^{ab}		0.0 ^b	
NAFU60	(+)	(+)	(+)	(-)	(-)	(+)	(+)	(-)
	0.2	0.2	0.0 ±	1.8	0.7	0.6 ±	1.7	2.8 ±
	±	±	0.0 ^c	±	±	0.4 ^a	±	0.9 ^{abc}
	0.0 ^{bc}	0.1 ^a		0.5 ^a	0.1 ^{ab}		0.0 ^c	
Gelose 50	(+)	(+)	(+)	(-)	(-)	(+)	(-)	(-)
	0.0	0.3	0.1 ±	0.8	1.2	4.4 ±	0.1	3.0 ±
	±	±	0.0 ^{abc}	±	±	0.4 ^{abc}	±	0.3 ^{abc}
	0.0 ^{bc}	0.2 ^a		0.1 ^a	0.1 ^{ab}		0.0 ^d	
Gelose 80	(+)	(+)	(+)	(-)	(-)	(+)	(+)	(-)
	0.2	0.6	0.3 ±	1.5	1.3	8.2 ±	0.5	4.5 ±
	±	±	0.1 ^{ab}	±	±	2.0 ^{bcd}	±	0.6 ^{bc}
	0.0 ^{bc}	0.4 ^a		0.0 ^a	0.2 ^b		0.2 ^d	
Hylon VII	(+)	(+)	(+)	(-)	(-)	(-)	(+)	(+)
	0.0	0.6	0.2 ±	1.3	1.1	8.7 ±	0.0	1.3 ±
	±	±	0.1 ^{abc}	±	±	3.1 ^{cd}	±	0.8 ^a
	0.0 ^c	0.4 ^a		0.4 ^a	0.2 ^{ab}		0.1 ^d	
AOBS	(+)	(+)	(+)	(-)	(-)	(+)	(+)	(+)
	0.7	1.3	0.3 ±	1.8	5.8	10.7	4.7	0.0 ±
	±	±	0.1 ^a	±	±	± 2.0 ^d	±	0.4 ^{ab}
	0.1 ^a	0.6 ^a		0.1 ^a	0.4 ^d		0.1 ^a	
HAWS	(+)	(+)	(+)	(-)	(-)	(-)	(+)	(-)
	0.2	1.0	0.3 ±	1.8	3.7	12.6	2.5	4.8 ±
	±	±	0.0 ^a	±	±	± 0.7 ^d	±	1.1 ^c
	0.1 ^b	0.5 ^a		0.4 ^a	0.3 ^c		0.0 ^b	
HAPS	(+)	(+)	(+)	(-)	(-)	(-)	(+)	(-)
	0.0	0.4	0.1 ±	0.9	0.3	2.9 ±	3.0	0.8 ±
	±	±	0.1 ^{abc}	±	±	2.1 ^{abc}	±	0.6 ^{abc}
	0.0 ^{bc}	0.2 ^a		0.3 ^a	0.2 ^a		0.4 ^b	

The differentiation values are calculated by the parameters of RS samples minus raw samples, (+) denotes an increase during digestion and (-) denotes a decrease. The actual values of each sample are listed in Table S3. Values are means ± standard deviation. Values with different letters in the same column are significantly different at $p < 0.05$, $n = 2$.

RC_X: relative amount of fraction X of debranched samples; ACL_X: average chain lengths (DP) of fraction X of debranched samples; fa: amylopectin chains with DP 6–12; fb₁: amylopectin chains with DP 13–24; fb₂: amylopectin chains with DP 25–36; fb₃: amylopectin chains with DP > 36.

behavior. During digestion, hydrolyzed products, including dextrin with short branches, are alongside with soluble glucose effectively removed, leading to a stimulated decrease in both α -1,6 and α -1,4 linkages. However, this explanation does not fully apply to HAPS, which exhibited a higher ratio of α -1,6 to α -1,4 linkages and longer side chains (Table S3). The relatively unaffected inner structure of HAPS RS resulted in negligible changes in the α -1,6 to α -1,4 linkage ratio due to (I) the smoother surface of HAPS compared to cereal starches, with fewer binding sites on the granular surface resulting in an “outside-in” pattern (Dhital, Warren, Butterworth, Ellis, & Gidley, 2015); and/or (II) potato starch containing fewer crystal defects than cereal starches, thereby limiting the hydrolysis of enzymes on the crystalline region (C. Li et al., 2020).

3.5. Helical order analysis

The quantitative analysis of solid starches using ¹³C NMR spectroscopy provided insights into the relative proportions of double (A, B-type) and single (V-type) helices changes during digestion (Table 4). The digestion process resulted in distinct changes in the helix percentages among the different HAS: (I) NAFU50 and NAFU60 exhibited a minor increase in both double and single helix relative contents. (II) Gelose 50, Gelose 80, HylonVII, and HAPS showed a reduction in both double and

single helix percentages. (III) In the case of AOBS and HAWS, there was a significant increase in the proportion of the double helix content, accompanied by a remarkable decrease in the single helix content.

These findings suggest that, during digestion, 1) NAFU50 and NAFU60 primarily undergo enzymatic breakdown of the amorphous starch molecules, while the double/single helical starch molecules remain relatively unaffected, as evidenced by the minor changes observed in AP CLD (section 3.3). It is noteworthy that these two HAMSs exhibited a high amount of short chains of amylopectin at DP 6–12, which facilitated the formation of defects within crystalline lamellae (Noda et al., 2009), which might be preferentially hydrolyzed during digestion. 2) Gelose 50, Gelose 80, HylonVII, and HAPS underwent enzymatic hydrolysis of both double and single helical starch structures, resulting in the dissociation of the helical structure, and the digestion of helical and non-helical regions occurred concurrently. (3) In AOBS and HAWS, a substantial reduction in the single helix content and a significant increase in the relative proportion of the double helix content were observed, which was related to the profound transformation of their molecular structures. The enzymatic hydrolysis process resulted in the complete degradation of both AM chains and long AP chains, yielding smaller remnants with DP ranging from 10 to 40 (Fig. 3). This degradation process has the potential to enhance both the rate and extent of AM aggregation into the double helix (Lopez-Rubio et al., 2008). The notable increase in double helix content observed in HAWS and AOBS, compared to other HAS granules, can be attributed to their higher amount and longer AM chains (AM_{2,3}), as the yield of such double helix structures is positively influenced by the length of the original AM chains (Eerlingen, Deceuninck, & Delcour, 1993).

Furthermore, the V-type single helix content exhibited greater changes during enzyme digestion compared with double helix content for all starches (Table S4), indicating that V-type helix was more susceptible to the hydrolytic enzymes.

3.6. Crystalline structure

All HAS granules showed a combination of B-type allomorph (peaks at 5.6, 17, 19.5, 22 and 24°) and V-type allomorph (peaks at 8, 13, 15, and 20°) (Fig. 5), in agreement with previous studies (Carcioli et al., 2012; H. Li et al., 2020b; Haiteng Li, Michael J. Gidley et al., 2019). The X-ray diffraction patterns of the starch granules were not impacted by digestion, but the disruption of crystals and the recrystallization were found during this process, which can be clearly observed from the changes of relative crystallinity of B-type allomorph and V-type allomorph (Table 4). Upon digestion, NAFU50, NAFU60, Gelose50, and HAPS mainly underwent a crystal disrupting process, as their total crystallinities decreased. However, the underlying mechanisms of the four starches were not the same. As discussed in section 3.5, the relative helix content of NAFU50 and NAFU60 was even enhanced, suggesting their crystals were not significantly affected.

Combining the increase in their branching degree (Table 4) and the decreased content of fb₁ chains in NAFU50 and fb₃ chains in NAFU60 (Table 4), it can be inferred that the enzymes primarily hydrolyzed the non-helical chains located in the crystalline lamella. Consequently, the decreased crystallinity observed in these two starches can be attributed to the disordered alignment of the double helix caused by the cleavage of connector chains between the backbone chains and the double helix in NAFU50, as well as the cleavage of the backbone chains in NAFU60. In comparison, the decreased crystallinity in Gelose 50 and HAPS can be simply explained by the destruction of the double helix motifs, as shown in section 3.5.

It is well known that the double helix content in starch granules is packed into crystals, thereby forming the semi-crystalline structure of starch granules (Zhong, Tai, et al., 2022). However, there may also be some dissociated double helices that are not packed with other double helices, known as “crystal defects” (Zhong, Liu, et al., 2020). The significant reduction in the double helix content and enhancement of

Table 4
Helix order (%), crystalline, and lamellar properties of different HAS granules.

Sample	α -1,6/ α -1,4 ratio	Single helix (%)	Double helix (%)	Amorphous (%)	Crystallinity (%)	% V-type crystallinity	% B-type crystallinity	FTIR ratio (1045/ 1022)	D (nm)	d _{ac} (nm)	d _a (nm)	d _c (nm)
NAFU50	(+)0.5 ± 0.0 ^{ab}	(+)1.4 ± 0.4 ^a	(+)0.9 ± 0.6 ^b	(-)2.0 ± 0.5 ^b	(-)17.2 ± 3.0 ^d	(-) 2.9 ± 0.0 ^c	(-) 14.3 ± 3.0 ^e	(+)0.0 ± 0.0 ^b	(+)0.3 ± 0.2 ^b	(+)0.6 ± 0.1 ^c	(+) 0.2 ± 0.0 ^a	(+)0.5 ± 0.1 ^{bc}
NAFU60	(+)0.7 ± 0.2 ^a	(+)1.5 ± 0.4 ^a	(+)0.6 ± 0.4 ^b	(-)2.1 ± 0.0 ^b	(-)5.1 ± 1.0 ^c	(-) 2.6 ± 0.2 ^{bc}	(-)2.5 ± 0.8 ^{cd}	(+)0.2 ± 0.0 ^b	(+)0.1 ± 0.0 ^b	(+)0.3 ± 0.1 ^c	(+) 0.1 ± 0.0 ^a	(+)0.0 ± 0.0 ^c
Gelose 50	(+)0.1 ± 0.0 ^{bc}	(-) 7.0 ± 1.0 ^b	(-) 8.5 ± 1.5 ^c	(+)16.1 ± 0.1 ^a	(-)7.6 ± 0.6 ^c	(-)2.3 ± 0.1 ^{bc}	(-)5.3 ± 0.7 ^d	(+)0.0 ± 0.0 ^b	(+)0.3 ± 0.0 ^b	(+)0.3 ± 0.0 ^c	(+) 0.1 ± 0.0 ^a	(+)0.2 ± 0.0 ^c
Gelose 80	(+)0.3 ± 0.2 ^{bc}	(-) 8.1 ± 0.4 ^b	(-) 7.4 ± 0.1 ^c	(+)15.5 ± 0.3 ^a	(+)1.0 ± 0.5 ^b	(-)0.5 ± 0.2 ^{ab}	(+)1.5 ± 1.0 ^{bc}	(+)0.0 ± 0.0 ^b	(+)0.7 ± 0.4 ^{ab}	(+)0.7 ± 0.4 ^{bc}	(+) 0.2 ± 0.0 ^a	(+)0.5 ± 0.2 ^{bc}
HylonVII	(+)0.3 ± 0.0 ^{bc}	(-) 7.9 ± 1.3 ^b	(-)7.1 ± 1.9 ^c	(+)15.1 ± 3.3 ^a	(+)5.4 ± 2.3 ^{ab}	(-)0.9 ± 0.4 ^{abc}	(+)6.2 ± 2.0 ^b	(+)0.2 ± 0.1 ^b	(+)0.2 ± 0.0 ^b	(+)0.2 ± 0.1 ^c	(+) 0.1 ± 0.0 ^a	(+)0.0 ± 0.0 ^c
AOBS	0.0 ± 0.0 ^c	(-) 12.2 ± 0.2 ^c	(+)24.5 ± 0.0 ^a	(-)12.3 ± 0.3 ^c	(+)8.2 ± 1.8 ^a	(-)7.0 ± 1.2 ^d	(+)13.7 ± 2.0 ^a	(+)1.3 ± 0.2 ^a	(+)1.4 ± 0.4 ^a	(+)1.5 ± 0.4 ^a	(-) 0.4 ± 0.1 ^b	(+)1.8 ± 0.4 ^a
HAWS	(+)0.5 ± 0.1 ^{ab}	(-) 11.5 ± 0.0 ^c	(+)25.4 ± 3.5 ^a	(-)14.0 ± 3.5 ^c	(+)6.0 ± 0.7 ^{ab}	(+)0.4 ± 0.2 ^a	(+)5.6 ± 0.5 ^b	(+)0.3 ± 0.0 ^b	(+)1.4 ± 0.2 ^a	(+)1.4 ± 0.2 ^{ab}	(+) 0.2 ± 0.0 ^a	(+)1.2 ± 0.1 ^{ab}
HAPS	0.0 ± 0.1 ^c	(-) 1.8 ± 0.8 ^a	(-)11.2 ± 3.0 ^c	(+)13.0 ± 1.2 ^a	(-)7.6 ± 0.8 ^c	(-)0.5 ± 0.0 ^{ab}	(-)7.1 ± 0.8 ^d	(-)0.1 ± 0.0 ^c	(-)0.3 ± 0.1 ^b	(+)0.3 ± 0.1 ^c	(+) 0.1 ± 0.0 ^a	(+)0.2 ± 0.1 ^c

The differentiation values are calculated by the parameters of RS samples minus raw samples, (+) denotes an increase during digestion and (-) denotes a decrease. The actual values of each sample are listed in Table S4.

The values are mean ± range for all parameters were calculated from duplicate measurements. Values with different letters in the same column are significantly different at $P < 0.05$, $n = 2$. Abbreviations are as follows: D, Bragg lamellar repeat distance; dac, da and dc, the thicknesses of total, amorphous, and crystalline lamellae, respectively.

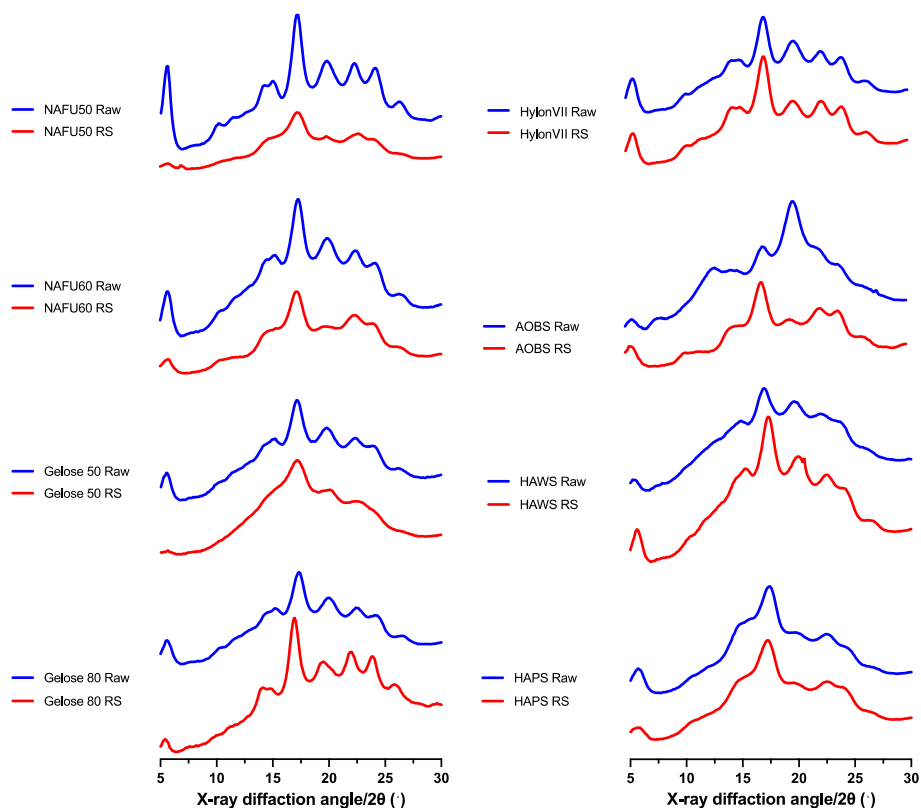


Fig. 5. X-ray diffraction (XRD) patterns and crystallinity of raw starches and resistant starch (RS).

crystallinity in Gelose 80 and HylonVII support this hypothesis. Hydrolytic attack on free double helices, combined with the hydrolysis of fb₁ chains (Table 3), leads to increased free space within the starch granules, facilitating the realignment and packing of remaining double helices and promoting the formation of crystal structures with fewer defects.

Additionally, the presence of newly generated ~2 nm remnants (Fig. 3B), resulting from the degradation of AM and long AP chains, further contributes to the formation of new double helices and crystal structures. This phenomenon was more significant in AOBS and HAWS, especially in AOBS, which had no AP molecules. In AOBS, the content of double helices increased by 24.5%, and the crystallinity increased by 13.7%. This implies that AM molecules synthesized from AP biosynthesis pathways with few branches, so-called “AM-like” molecules (Zhong, Tai, et al., 2022), had a strong capacity to form new double helices and crystal structures upon digestion, by being severely degraded into remnants with a size of approximately 2 nm.

3.7. Lamellar structure

The synchrotron SAXS data (Fig. 6) and the fitted parameters (Table 4) primarily indicate the following: (I) broadening of the 9 nm lamellar peak following digestion (Fig. 6B), suggests increased polydispersity of all HAS granules upon digestion; (II) thickening of the average thicknesses of the semi-crystalline lamellae (D) is mainly due to the expansion of the thicknesses of crystalline lamellae (d_c) (Table 4), which results from the hydrolysis of AP connector chains (fb₁) (Fig. 4) and the distance between backbone chains and double helices. These findings support the previous discussion that increased space allows for greater mobility of starch molecules in the crystalline lamellae, thereby promoting the realignment and packing of the double helix structure.

3.8. Surface order degree

FTIR-ATR analysis was employed to investigate the granular surface order degree, as this analytical method is known for its sensitivity towards alterations in short-range order, including chain conformation and helicity, particularly within the surface (2 μm) region (Sevenou,

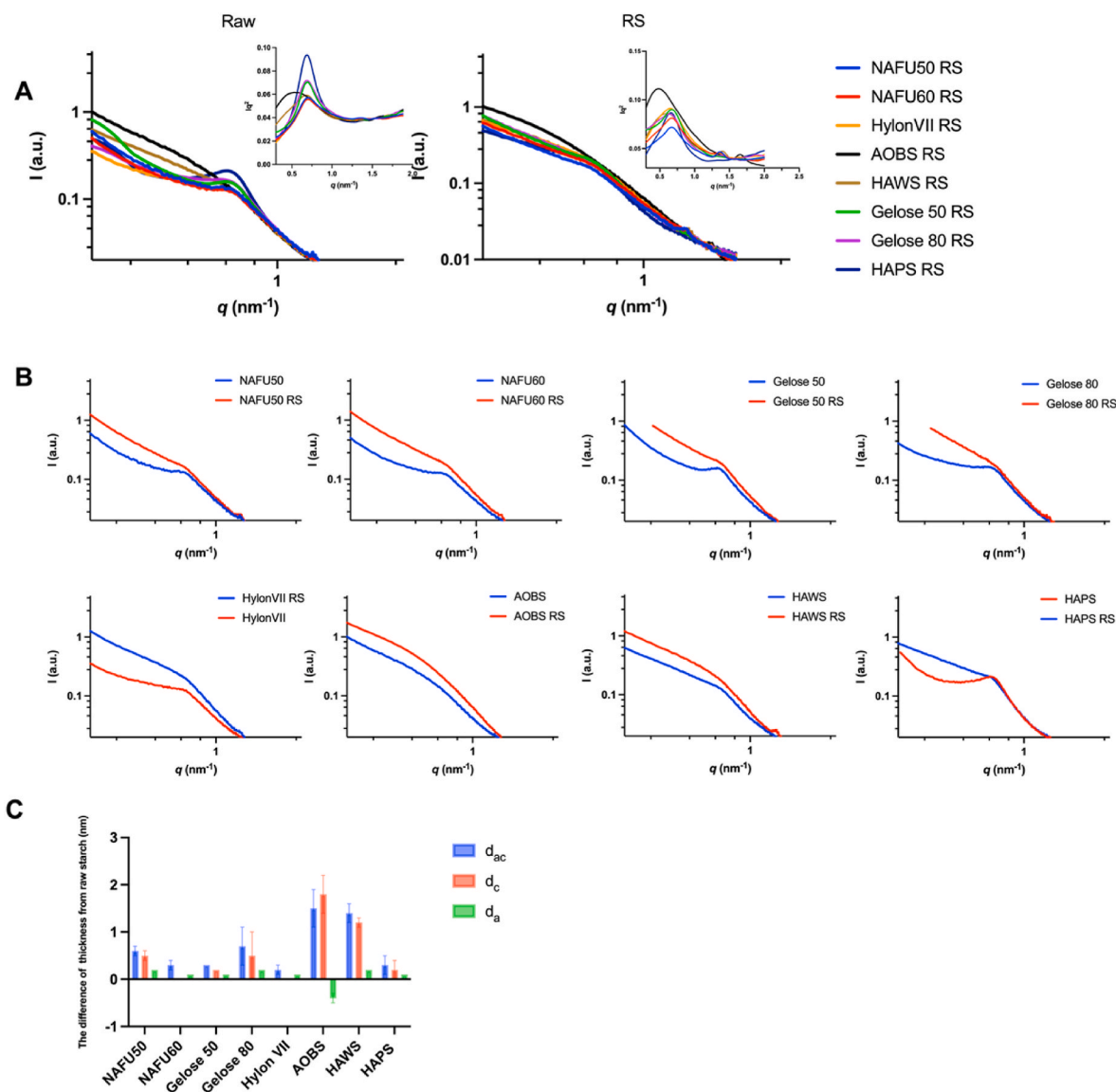


Fig. 6. Small-angle X-ray scattering (SAXS) profiles of raw starch and resistant starch (RS) (A); comparison of profiles between raw starch and RS (B); changes in thickness parameters (RS-Raw) for the semi-crystalline lamellae (including d_{ac}, d_a, and d_c, which represent the thicknesses of the total, amorphous, and crystalline lamellae, respectively) (C).

Hill, Farhat, & Mitchell, 2002). The 1045/1022 cm^{-1} ratio exhibited varied levels of increase for all HAS granules except for HAPS (Table 4), suggesting an increase in molecular order within the surface region as hydrolysis progressed (Lopez-Rubio et al., 2008). Interestingly, the changes observed in the FTIR-ATR data did not fully align with the results obtained from XRD and ^{13}C NMR analysis, implying different structural evolutions between the surface and inner regions of the various types of HAS granules.

It has been proposed that AM is more concentrated at the periphery of the granules than in the core (Pan & Jane, 2000), and the degradation of AM chains in HAS granules facilitated the reorganization of the surface region of the RS remnants. However, this reorganization phenomenon was not observed in HAPS, which exhibited a decreased 1045/1022 cm^{-1} ratio, indicating a decrease in the surface order degree. This can be attributed to the lower AM content and the presence of a well-organized yet less flexible surface structure of HAPS.

3.9. Morphology

The morphology of HAS granules and their RS residues, as depicted in Fig. 7 and Fig. S4, showed two distinct observations: (I) a reorganization of the granular structure in most granules of AOBs and HAWs, and (II) the formation of porous and/or cracked granular structures in partial granules of the other six types of HAS granules upon digestion. Combining these findings with the digestion profiles (Fig. 2B), it is

interesting to note that the reorganized structure of RS residues in AOBs and HAWs, composed of conglomerated small granules in “sheaths” (Shaik et al., 2016) was highly resistant to digestion, indicating that AM reorganization upon digestion increased its hydrolytic resistance. Further, the data from other structural levels and the discussion above suggest that the digestive resistance of these regenerated granules can be attributed to the recrystallization of cleaved starch molecules in a loose crystalline lamellar structure, resulting in the generation of more double helical and B-type crystals.

However, for the rest of the HAS granules, including all the HAMSs and the HAPS, the digestion pattern within the same preparation was markedly heterogeneous. Some granules appeared to be unaffected by amylases, while others were significantly digested, in agreement with previous data (Shrestha, Jaroslav, et al., 2012). In particular, some granules among the HAMSs were almost completely hydrolyzed along the channels, forming large holes deeper into the granules through “endo corrosion” (indicated by red arrows in Fig. 7B), whereas other granules were only affected on the surface (blue arrow). Additionally, smaller and intermediate-sized starch granules were found to be more resistant to the erosion of digestive enzymes than larger granules (Hoover & Sosulski, 1985). Similarly, HAPS exhibited a heterogeneous digestion pattern, with many granules showing only superficial surface erosion and cracks, while their RS maintained a granular shape similar to that of native starches (Fig. S4). These findings underscore the heterogeneous nature of hydrolytic resistance in starch granules. It is

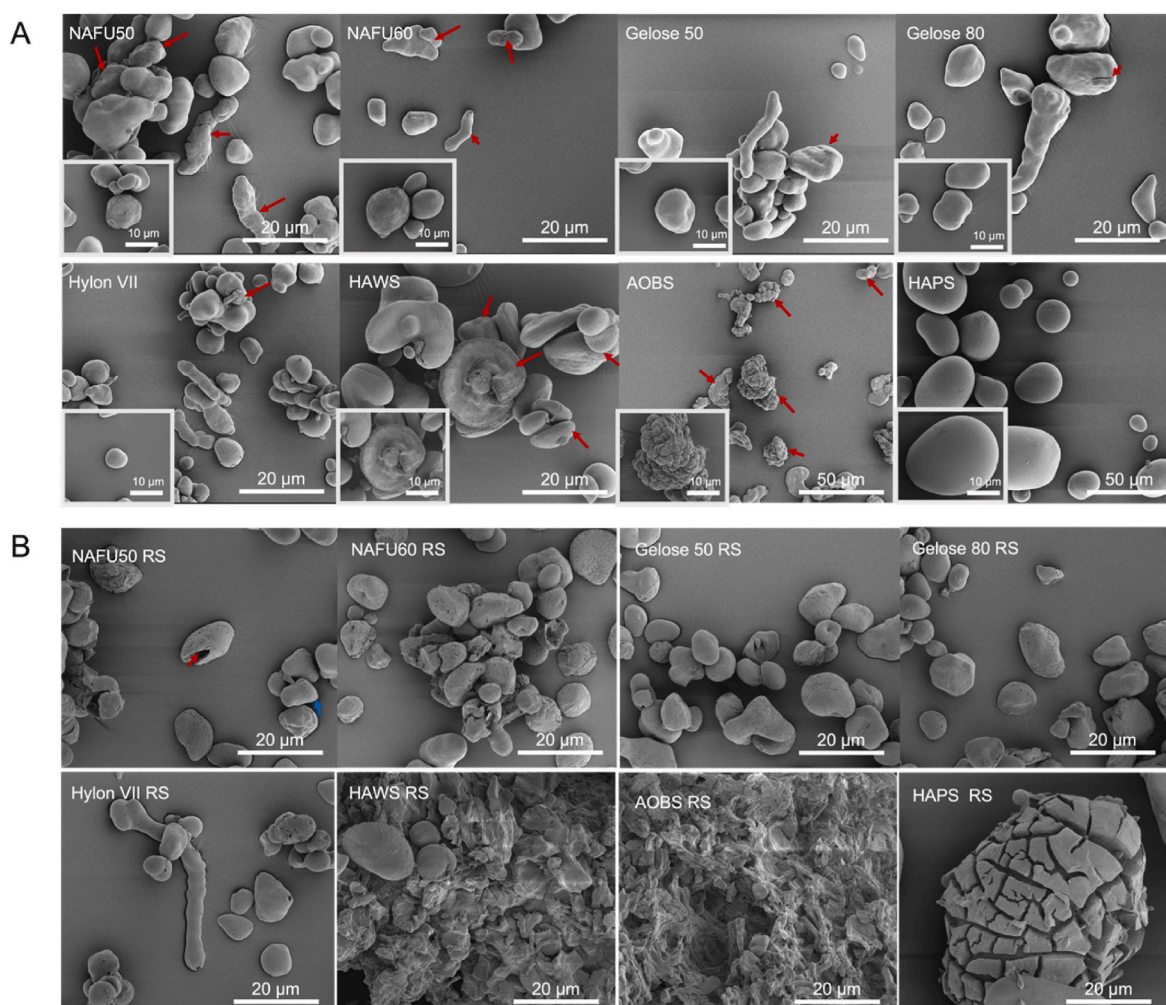


Fig. 7. Scanning electron microscopy (SEM) images comparing native granules (A) with corresponding resistant starch (RS) (B) after 10 h of *in vitro* digestion. While the majority of the high-amylose starches (HAS) exhibit a relatively smooth surface without apparent channels, noteworthy variations in distribution were observed within a single HAS sample. Some granules exhibited a more rugged and fragile appearance, as highlighted by the red arrows in (A).

hypothesized that the presence of granules with varying organization and surface smoothness (Fig. 7A), along with differences in the accessibility of binding sites on the granular surface among different granules (Tian, Wang, et al., 2023) within a single high AM starch (HAS) sample, likely contributes to the observed variations in digestion behavior within the same starch specimen. Additionally, the percentage of such fragile granules within a single HAS sample may impact the overall RS content. However, due to the limitations of the technique used to separate and track single granules, fully understanding the underlying mechanisms remains challenging.

4. Discussion

4.1. What type of structures control digestibility of HAS?

The HAS granules examined in this study possess, following prolonged hydrolysis, significantly higher resistant starch (RS) content (>20%) compared to regular starch granules (waxy maize starch and normal maize starch) (<5%). These findings provide a deeper understanding of the underlying mechanisms of starch digestion, which is crucial for advancing human nutrition and health. Based on the 180 min degree of digestibility and RS content, the hydrolytic resistance of the

HAS granules can be ranked as follows: HAPS > Gelose 50, Gelose 80, Hylon VII > NAFU50, NAFU60 > AOBS, HAWS. To further explore factors influencing digestibility, a correlation analysis between eight native starch granule structural parameters and their respective digestibility was conducted (Fig. 8A).

Based on the findings presented in this study, it can be concluded that the architectural characteristics of starch granules play a pivotal role in determining the substantial differences in enzyme susceptibility between low to moderate AM starch (comprising waxy and normal AM content starch) and HAS. While it is noteworthy that certain HAS granules exhibit a rough and uneven surface, they do not possess the pores and channels typically observed on the surfaces of WMS and NMS. It is probable that the presence of surface pores, a common feature of normal cereal starch, facilitates enzyme access by expanding during digestion, allowing for rapid penetration into the less-organized core of the granule (Blazek & Gilbert, 2010). In contrast, HAS granules lack extensive surface pores, necessitating enzyme digestion to progress from the outside inward. The outer regions of the granules serve as an effective barrier, limiting enzyme access to the less organized interior. Although the reduced presence of surface pores, resulting in limited enzyme attack sites (Tian, Wang, et al., 2023), likely contributes significantly to the resistance of HAS, the precise mechanisms

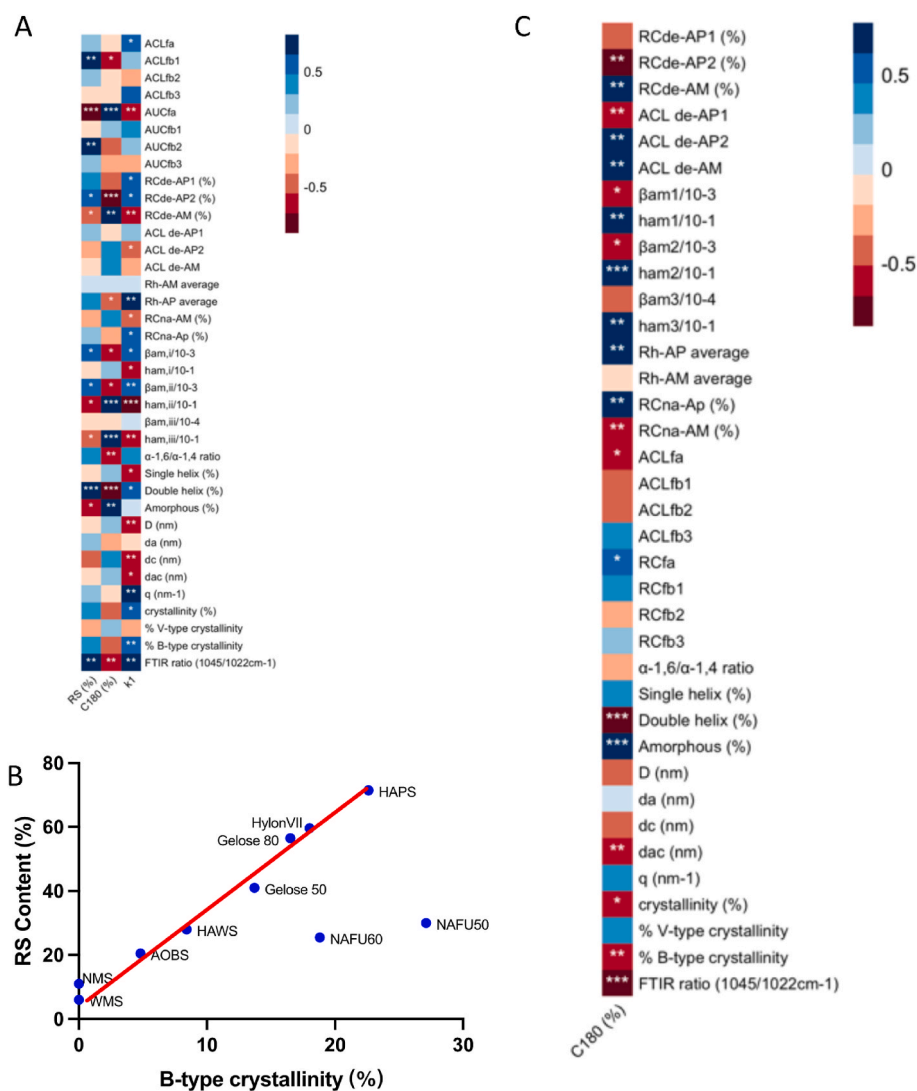


Fig. 8. Correlation analysis of the A) native starch granule structural parameters and digestibility; B) the relationship between B-type crystallinity and RS content of HAS (the linear fitting ($r^2 = 0.98$) excluding NAFU50 and NAFU60); C) changes of digestion percentage and structural parameters between native starch granules and resistant starch (RS) (RS-Raw).

underlying this phenomenon remain less understood. It is tempting to speculate that the presence of B-type crystals is responsible for the smooth surface and enhanced resistance observed in HAS. This speculation is based on the notion that B-type crystals tend to form larger-sized blocklets at the periphery (D. Gallant, Bouchet, Buleon, & Perez, 1992; Pérez & Bertoft, 2010), to a depth of approximately 10 μm . These blocklets are believed to play a crucial role in conferring resistance to hydrolysis in HAS granules (D. Gallant et al., 1992). Additionally, a notable positive correlation is observed between B-type crystallinity and the content of RS, with the exception of NAFU50 and NAFU60 in this context (Fig. 8B). Furthermore, the reorganization of HAS, as seen in AOBS and HAWS during digestion, leads to the formation of B-type crystallinity, thereby augmenting resistance.

However, B-type crystallinity alone cannot fully account for the resistance observed in HAS, as exemplified by NAFU50 and NAFU60, which do not strictly follow the expected positive relationship between B-type crystallinity and resistance (Fig. 8B). As evident from SEM observations (Fig. 7A), the distribution of granules within the same starch type is not uniform. Some granules appear smoother, while others exhibit a rougher and seemingly fragile texture. Consequently, some granules remain intact after digestion, while others are destroyed (Fig. 7B). As judged from inspection of the HAS granule images, HAWS and AOBS contain the most rough granules and follow NAFU50 and NAFU60 in this regard. Gelose 50, 80, and Hylon VII display intermediate characteristics, with more smooth granules, while HAPS appears to have the most smooth granules. This order, albeit no precise measurements of the surface roughness were obtained, aligns with the digestibility patterns. Among HAMS, this non-uniform distribution appears more pronounced in NAFU50 and NAFU60, where significant variation in the presence of rough and smooth granules is observed, potentially contributing to their lower RS content. It would be intriguing to separate and analyze these fragile granules individually, as the crystallinity values presented here represent averages for specific starch types. However, such separation poses practical challenges. Therefore, it appears that the percentage of smooth granules within HAS also plays a crucial role in determining their overall resistance. Nonetheless, the reasons behind the observed uneven distribution within HAS remain unclear.

Furthermore, the localization of AM within the granules and its interaction with amylopectin can influence local packing, which, in turn, impacts hydrolytic resistance (Blazek & Gilbert, 2010; Gallant, Bouchet, & Baldwin, 1997). The organization of AM, whether separate or mixed with amylopectin, remains uncertain. In non-HAS, AM is often considered largely free of interactions with amylopectin or other AM chains, as indicated by the fact that amylopectin retains its crystallinity while AM mostly leaches out below the gelatinization temperature (Ring, l'Anson, & Morris, 1985). However, it has been suggested that in HAS, AM may participate in the short-range order by forming double helices with AP side chains or with other AM molecules (Zhong, Liu, et al., 2020). Additionally, while the exact location of AM within HAS remains uncertain, there are indications that AM chains tend to be more concentrated in the periphery of starch granules, particularly in HAS (Blennow et al., 2020; Kuakpetoon & Wang, 2007). Hence, the fine structure of AM could be a critical factor in determining the surface local organization of HAS. As indicated by Pearson correlation analysis (Fig. 8A), short-range order characteristics such as the content of double helices and surface order degree (as indicated by FTIR) vary among different HAS granules due to differences in AM and amylopectin fine structures and botanical origins, and these variations might contribute to differences in resistance among HAS.

The presence of higher amounts of short chains (fa) can negatively affect the ordering of crystalline structures by creating defects (Koroteeva et al., 2007). Therefore, having fewer and longer fa chains may contribute to resistance by supporting the formation of double helices. Furthermore, shorter AM₁ and AM₂ chains may lead to higher resistance by promoting co-organization with amylopectin side chains (Zhong, Liu,

et al., 2020), while longer and higher amounts of AM₃, which have the potential to disrupt the formation of double helical segments and crystal structures, might contribute to lower resistance. Thus, among HAS starches, those with longer and fewer fa chains, shorter AM₁ and AM₂ chains, and more AM₁, while having fewer long AM chains (AM₂ and AM₃), are likely to be contribute to more tight interactions at the granular periphery and resistance to amylase-assisted hydrolysis.

4.2. Structural changes during digestion

The findings of the study revealed that the HAS granules can be grouped into two distinct categories based on their structural changes during digestion. The first group, consisting of HAMSs and HAPS granules, had relatively high RS content and varying AM content, and exhibited minimal structural changes during the digestion process. The second group, which included AOBS and HAWS, experienced significant structural changes from the molecular level to the granular level during digestion.

The primary factor that contributed to the low extent of structural changes in HAMS and HAPS starches, in comparison to the pronounced changes in HAWS and AOBS, was found at the granular surface. As mentioned above, the absence of pores and channels of most granules restricts enzyme access to HAMS and HAPS substrates. Conversely, the susceptible surface of HAWS and AOBS permit enzyme entrance to the granular matrix, leading to a significant influence on the inner structure in comparison to other starches. However, the less ordered surface structure of HAWS and AOBS provided more flexibility to their chains, allowing for reorganization and increased surface order during digestion. A similar reorganization process also occurs for HAMS starches, where flexible AM molecules are enriched on the surface. However, this is not the case for HAPS starches, as the degree of surface order decreases during digestion due to the low AM content and highly well-organized surface, which reduces flexibility and limits reorganization.

The inner structure of AOBS and HAWS starches exhibits a higher degree of flexibility and disordered arrangement, as discussed above, allowing for increased possibility of dynamic reorganization and chain alignments. The newly formed segments and single remnants of these starches, specifically the dextrin with a single peak at Rh \sim 2 nm, pack to form a higher content of double helix (3–5 times) and B-type crystallinity (2–4 times) in the AOBS and HAWS RS, leading to a more resistant structure within both semi-crystalline and amorphous regions. Interestingly, this formation size (\sim 2 nm) is consistent across various sources of HAS, despite variations in molecular size distribution. Notably, a relatively high amount of this fraction was found in Hylon VII and Gelose 80, which have higher AM content. For HAMS, there also exists a competition between the organized structure, which provides high resistance to enzymes but reduces flexibility, and reorganization ability. Starches with a more flexible inner structure, such as NAFU50 and NAFU60, which have a higher amount of longer AM chains (AM_{2,3}), lower degree of branching (DB), and lower helix content, exhibited a greater reorganization ability with increased helix content. On the contrary, HylonVII and Gelose 80, which had a less flexible structure, showed a decreased helix content. However, there was an increased crystallinity due to the increased free space during digestion, resulting in a rearrangement of existing double helices or the newly formed \sim 2 nm fractions. On the contrary, HAPS and Gelose 50 showed no new chain interactions or packing during digestion, resulting in decrease in both helix content and crystallinity. This lack of structural reorganization might be attributed to their well-organized structure and relatively low AM content (high AP content), which limits flexibility and provides fewer AM chains for reorganization.

The findings suggest that the hydrolysis process can reduce steric restrictions and promotes a decrease in chain length of molecules within HAS, resulting in the formation of \sim 2 nm segments, which exhibit the potential to undergo double helix formation and rearrangement. Notably, the flexible inner structure and high AM content of HAS

contribute to an increased likelihood of these novel chain interactions and organization taking place during the digestion process.

4.3. Enhanced resistant starch (eRS)

While the resistance mechanism of HAS granules is considered to be consistent with that of the B-type crystalline polymorph, supposedly related to a smooth granule surface, provides an effective barrier for the entry of enzymes to the granular matrix (Shrestha, Jaroslav, et al., 2012) causing less effective attack sites for digestive enzymes (Tian, Wang, et al., 2023). The direct comparison of the dynamic morphological and structural changes of different HASs and their resistant starch (RS) residues also suggests that the digestion of HAS granules involves the existing resistant architecture and flexible reorganization (Fig. 9) (Table 5).

In contrast to typical HASs, AOBS and HAWS, similar to HAS from pea (70% AM) (Warren, Butterworth, & Ellis, 2013), lack the smooth surface and are instead composed of highly disordered α -glucan chains that are readily hydrolyzed, resulting in fast digestion in the first 4 h. However, after 10 h of digestion, a significant fraction (20–30%) of these starches remains, and these fractions exhibit high resistance (\sim 90%) (Fig. 2C), which can be termed as enhanced resistant starch (eRS). This effect has also been observed in germinated AOBS grain, i.e. fast initial hydrolysis followed by increased hydrolytic resistance of the endosperm granules (Shaik et al., 2014).

The longer and flexible AM chains in the loose structure of HAWS and AOBS are more likely to be entirely cleaved into chains of lengths that can form helices. The reduction in AM chain length to around DP 90 promotes AM aggregation, leading to an increase in both the rate and amount of aggregation, and recrystallization (Gidley & Bulpin, 1989).

Complete alignment of the polymer chains is not possible under normal crystallization conditions due to entropic reasons (high entropic favoring disorderly, random configurations), while it was proposed that the RS (crystalline structure) formation occurs due to the aggregation of AM helices over a specific region of the chain, which is approximately 24 glucos residues, 4 helix turns, and 8.4 nm (Eerlingen et al., 1993). This is consistent with the dextrin found in eRS here (DP \sim 20–30, \sim Rh 2 nm) and thicker crystal lamellae (8.5–9.3 nm). Therefore, the formation of eRS in HAWS and AOBS is attributed to the hydrolysis of AM during digestion, which induces retrogradation by accelerating the rate of crystallization and optimizing the length of the fragments that can align in a crystalline form. It is interesting to note that the reorganization of HASs during digestion has also been observed before, along with the resulting structure of DP 10–30 dextrin (Haiteng Li et al., 2022; Lopez-Rubio et al., 2008), but this effect is even more pronounced for HAWS and AOBS in our study. Additionally, previous studies have demonstrated that only a portion of these reorganized starches (41–45%) exhibit resistance to a second round of *in vitro* digestion (Lopez-Rubio et al., 2008), whereas we report a much higher resistance (90%) in eRS.

The reorganized surface structure and the formation of newly formed 2 nm segments, which lead to a high double helix or increased crystallinity in HAMS RS, within the “trimmed” inner part affected by digestive enzymes, contributed to similar or slightly decreased digestibility compared to its raw starch. On the contrary, the absence of a reorganized surface structure and a decrease in the ordered inner structure in HAPS RS resulted in a significant reduction in its resistance, in agreement with the very small amount of the 2 nm segments found in its RS remnants.

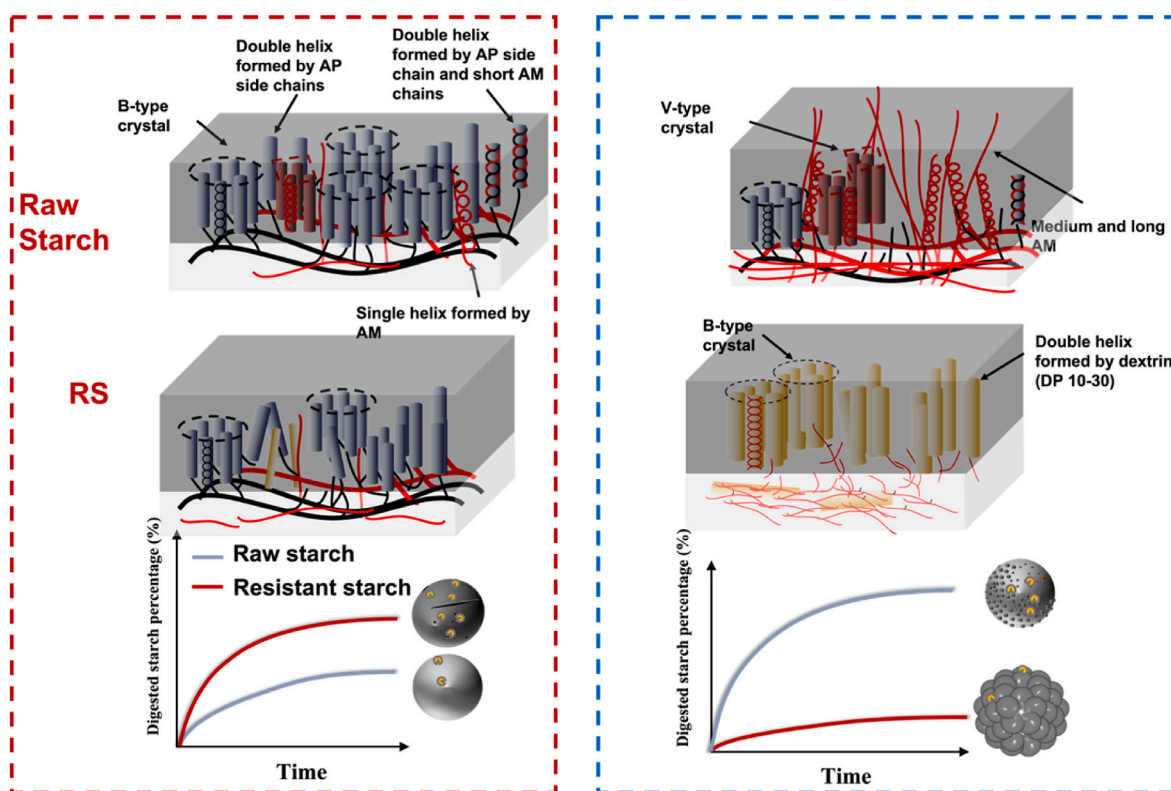


Fig. 9. Plausible comparative model of structure and digestibilities of HAMS and HAPS (left), and AOBS and HAWS (right). The HAMS and HAPS exhibit a well-organized granular structure and a higher amount of double helix, with an ordered lamellar structure that is favored by longer fa , fb_1 , shorter $AM_{1,2}$, and fewer AM_3 . These properties result in high hydrolysis resistance but less flexibility and a reduced ability to form new ordered structures during digestion. On the other hand, HAWS and AOBS, representing temperate cereal starch types, have a loose granular surface and a defect lamellar organization caused by more and shorter fa , short fb_1 , longer $AM_{1,2}$, and a high amount of AM_3 . The higher flexibility causes less RS while favoring the generation of more organized double helix structures by reducing the chain length, which is highly hydrolytically resistant.

Table 5
Structure features, hydrolysis resistance, and reorganization ability during digestion of different HAS granules.

Starches	Granular surface	Inner supramolecular structure	Molecular structure	Resistant ability	Reorganized ability
NAFU50, NAFU60 Gelose50, Gelose80, HylonVII	Most granules with smooth surface	Low double/single helix content High double/single helix content	High amount of fa, AM _{2,3} High amount and long AP ₂ ; less fa; high amount AM ₁	Medium High	Medium Medium
AOBS, HAWS	Most granules with rough surface	Low double helix content and crystallinity	High amount and short fa; high amount and long AM _{2,3}	low	High
HAPS	Extremely smooth surface and highest surface order degree	High crystallinity and double helix content, less single helix	Less AM, short AP ₂	High	Low

5. Conclusion

Our investigation underscores that the resistance of various high AM starches (HASs) to hydrolytic degradation cannot be solely attributed to their AM content. Instead, the percentage of smooth surfaces granules, potentially linked to the formation of large blocklets through B-type crystalline polymorphism, and locally organized structure with a high double helix content, plays a pivotal role in determining their resistance. High AM wheat starch (HAWS) and AM-only barley starch (AOBS), with longer AM chains and short branch chains (fa), exhibit loose structures and lower resistance to enzymatic hydrolysis. However, these structures allow for higher reorganization ability during digestion, resulting in the formation of enhanced resistant starch (eRS) that is only partially hydrolyzed (10%) during the second round of *in vitro* digestion. In contrast, high AM maize starch (HAMS) and high AM potato starch (HAPS) demonstrate higher percentage of smooth granules and resistant starch content but lower reorganization ability during digestion. Certain HAS varieties demonstrated the highest level of enhanced resistance during digestion, suggesting the potential for developing starches with similar reorganization ability. The granular surface organization is crucial for the hydrolytic resistance of HAS; however, the exact mechanism by which it prevents interaction with digestive enzymes remains unclear. Further advanced studies may shed light on the complex interactions between starch surface structures and digestive enzymes.

Author statement

Yu Tian: Conceptualization, Investigation, Methodology, Software, Writing - Original Draft, Writing - Review & Editing.

Bent Larsen Petersen: Resources, Writing - Review & Editing.

Xingxun Liu: Methodology, Writing - Review & Editing.

Haiteng Li: Methodology, Writing - Review & Editing.

Jacob Judas Kain Kirkensgaard: Investigation, Writing - Review & Editing.

Kasper Enemark-Rasmussen: Investigation, Writing - Review & Editing.

Bekzod Khakimov: Investigation, Writing - Review & Editing.

Kim Henrik Hebelstrup: Resources, Writing - Review & Editing.

Yuyue Zhong: Conceptualization, Conceptualization, Supervision, Resources, Writing - Review & Editing.

Andreas Blennow: Conceptualization, Supervision, Funding acquisition, Writing - Review & Editing.

Declaration of competing interest

The authors declare no competing financial interest.

Data availability

No data was used for the research described in the article.

Acknowledgments

Yu Tian gratefully acknowledges the support of the China

Scholarship Council (CSC) funding (#202003250068) for her PhD studies at the University of Copenhagen (UCPH), Denmark. Xingxun Liu acknowledges the grants from the National Natural Science Foundation of China (32372476).

Appendix A. Supplementary data

Supplementary data to this article can be found online at <https://doi.org/10.1016/j.foodhyd.2023.109593>.

References

- Blazek, J., & Gilbert, E. P. (2010). Effect of enzymatic hydrolysis on native starch granule structure. *Biomacromolecules*, *11*(12), 3275–3289.
- Blennow, A., Bay-Smidt, A. M., Wischmann, B., Olsen, C. E., & Møller, B. L. (1998). The degree of starch phosphorylation is related to the chain length distribution of the neutral and the phosphorylated chains of amylopectin. *Carbohydrate Research*, *307*(1–2), 45–54.
- Blennow, A., Skryhan, K., Tanackovic, V., Kronic, S. L., Shaik, S. S., Andersen, M. S., ... Nielsen, K. L. (2020). Non-GMO potato lines, synthesizing increased amylose and resistant starch, are mainly deficient in isoamylase debranching enzyme. *Plant Biotechnology Journal*, *18*(10), 2096–2108.
- Blennow, A., Wischmann, B., Houborg, K., Ahmt, T., Jørgensen, K., Engelsen, S. B., ... Poulsen, P. (2005). Structure function relationships of transgenic starches with engineered phosphate substitution and starch branching. *International Journal of Biological Macromolecules*, *36*(3), 159–168.
- Carciofi, M., Blennow, A., Jensen, S. L., Shaik, S. S., Henriksen, A., Buléon, A., ... Hebelstrup, K. H. (2012). Concerted suppression of all starch branching enzyme genes in barley produces amylose-only starch granules. *BMC Plant Biology*, *12*(1), 223.
- Dhital, S., Warren, F. J., Butterworth, P. J., Ellis, P. R., & Gidley, M. J. (2015). Mechanisms of starch digestion by α -amylase-structural basis for kinetic properties. *CRC Critical Reviews In Food Technology*, *57*(5), 875–892.
- Edwards, C. H., Grundy, M. M., Grassby, T., Vasilopoulou, D., Frost, G. S., Butterworth, P. J., ... Ellis, P. R. (2015). Manipulation of starch bioaccessibility in wheat endosperm to regulate starch digestion, postprandial glycemia, insulinemia, and gut hormone responses: A randomized controlled trial in healthy ileostomy participants. *The American Journal of Clinical Nutrition*, *102*(4), 791–800.
- Edwards, C. H., Warren, F. J., Milligan, P. J., Butterworth, P. J., & Ellis, P. R. (2014). A novel method for classifying starch digestion by modelling the amylolysis of plant foods using first-order enzyme kinetic principles. *Food & Function*, *5*(11), 2751–2758.
- Erlingen, R. C., Deceuninck, M., & Delcour, J. A. (1993). Enzyme-resistant starch. II. Influence of amylose chain length on resistant starch formation. *Cereal Chemistry*, *70*(3), 345–350.
- Evans, A. (2016). Resistant starch and health. In *Encyclopedia of food grains* (pp. 230–235).
- Evans, A., & Thompson, D. B. (2008). Enzyme susceptibility of high-amylose starch precipitated from sodium hydroxide dispersions. *Cereal Chemistry*, *85*(4), 480–487.
- Gallant, D. J., Bouchet, B., & Baldwin, P. M. (1997). Microscopy of starch: Evidence of a new level of granule organization. *Carbohydrate Polymers*, *32*(3–4), 177–191.
- Gallant, D., Bouchet, B., Buleon, A., & Perez, S. (1992). Physical characteristics of starch granules and susceptibility to enzymatic degradation. *European Journal of Clinical Nutrition*, *46*(2), 3–16.
- Gidley, M. J., & Bulpin, P. V. (1989). Aggregation of amylose in aqueous systems: The effect of chain length on phase behavior and aggregation kinetics. *Macromolecules*, *22*(1), 341–346.
- Hoover, R., & Sosulski, F. (1985). Studies on the functional characteristics and digestibility of starches from *Phaseolus vulgaris* biotypes. *Starch Staerke*, *37*(6), 181–191.
- Ishikawa, K., Matsui, I., Honda, K., & Nakatani, H. (1990). Substrate-dependent shift of optimum pH in porcine pancreatic α -amylase-catalyzed reactions. *Biochemistry*, *29*(30), 7119–7123.
- Khakimov, B., Mobaraki, N., Trimigno, A., Aru, V., & Engelsen, S. B. (2020). Signature Mapping (SigMa): An efficient approach for processing complex human urine 1H NMR metabolomics data. *Analytica Chimica Acta*, *1108*, 142–151.

- Kong, X., Zhu, P., Sui, Z., & Bao, J. (2015). Physicochemical properties of starches from diverse rice cultivars varying in apparent amylose content and gelatinisation temperature combinations. *Food Chemistry*, *172*, 433–440.
- Koroteeva, D. A., Kiseleva, V. I., Krivandin, A. V., Shatalova, O. V., Błaszczak, W., Bertoft, E., ... Yuryev, V. P. (2007). Structural and thermodynamic properties of rice starches with different genetic background: Part 2. Defectiveness of different supramolecular structures in starch granules. *International Journal of Biological Macromolecules*, *41*(5), 534–547.
- Kuakpetoon, D., & Wang, Y.-J. (2007). Internal structure and physicochemical properties of corn starches as revealed by chemical surface gelatinization. *Carbohydrate Research*, *342*(15), 2253–2263.
- Kuang, Q., Xu, J., Liang, Y., Xie, F., Tian, F., Zhou, S., et al. (2017). Lamellar structure change of waxy corn starch during gelatinization by time-resolved synchrotron SAXS. *Food Hydrocolloids*, *62*, 43–48.
- Li, H., Dhital, S., Flanagan, B. M., Mata, J., Gilbert, E. P., & Gidley, M. J. (2020a). High-amylose wheat and maize starches have distinctly different granule organization and annealing behaviour: A key role for chain mobility. *Food Hydrocolloids*, *105*, Article 105820.
- Li, H., Dhital, S., Flanagan, B. M., Mata, J., Gilbert, E. P., & Gidley, M. J. (2020b). High-amylose wheat and maize starches have distinctly different granule organization and annealing behaviour: A key role for chain mobility. *Food Hydrocolloids*, Article 105820.
- Li, H., Dhital, S., Flanagan, B. M., Mata, J., Gilbert, E. P., Gilbert, R. G., et al. (2022). Amorphous packing of amylose and elongated branches linked to the enzymatic resistance of high-amylose wheat starch granules. *Carbohydrate Polymers*, *295*, Article 119871.
- Li, R., Ding, L., Guo, K., Qu, J., Herburger, K., Persson, S., ... Zhong, Y. (2023). The effects of different types of high-amylose maize starches on viscosity and digestion of acidified milk gels. *Food Chemistry*, *404*, Article 134525.
- Li, H., Gidley, M. J., & Dhital, S. (2019a). High-amylose starches to bridge the “fiber gap”: Development, structure, and nutritional functionality. *Comprehensive Reviews in Food Science and Food Safety*, *18*(2), 362–379.
- Li, H., Gidley, M. J., & Dhital, S. (2019b). High-amylose starches to bridge the “fiber gap”: Development, structure, and nutritional functionality. *Comprehensive Reviews in Food Science and Food Safety*, *18*(2), 362–379.
- Li, H., Gidley, M. J., & Dhital, S. (2019c). High-amylose starches to bridge the “fiber gap”: Development, structure, and nutritional functionality. *Comprehensive Reviews in Food Science and Food Safety*, *18*(2), 362–379.
- Li, C., Gong, B., Hu, Y., Liu, X., Guan, X., & Zhang, B. (2020). Combined crystalline, lamellar and granular structural insights into in vitro digestion rate of native starches. *Food Hydrocolloids*, *105*, Article 105823.
- Li, L., Jiang, H., Campbell, M., Blanco, M., & Jane, J.-I. (2008). Characterization of maize amylose-extender (ae) mutant starches. Part I: Relationship between resistant starch contents and molecular structures. *Carbohydrate Polymers*, *74*(3), 396–404.
- Li, H., Prakash, S., Nicholson, T. M., Fitzgerald, M. A., & Gilbert, R. G. (2016). The importance of amylose and amylopectin fine structure for textural properties of cooked rice grains. *Food Chemistry*, *196*, 702–711.
- Liu, G., Gu, Z., Hong, Y., Wei, H., Zhang, C., Huang, S., ... Li, Y. (2020). Effects of molecular interactions in debranched high amylose starch on digestibility and hydrogel properties. *Food Hydrocolloids*, *101*, Article 105498.
- Lopez-Rubio, A., Flanagan, B. M., Shrestha, A. K., Gidley, M. J., & Gilbert, E. P. (2008). Molecular rearrangement of starch during in vitro digestion: Toward a better understanding of enzyme resistant starch formation in processed starches. *Biomacromolecules*, *9*(7), 1951–1958.
- Man, J., Yang, Y., Zhang, C., Zhang, F., Wang, Y., Gu, M., ... Wei, C. (2013). Morphology and structural characterization of high-amylose rice starch residues hydrolyzed by porcine pancreatic α -amylase. *Food Hydrocolloids*, *31*(2), 195–203.
- Morita, T., Ito, Y., Brown, I. L., Ando, R., & Kiriya, S. (2007). In vitro and in vivo digestibility of native maize starch granules varying in amylose contents. *Journal of AOAC International*, *90*(6), 1628–1634.
- Nada, S. S., Zou, W., Li, C., & Gilbert, R. G. (2017). Parameterizing amylose chain-length distributions for biosynthesis-structure-property relations. *Analytical and Bioanalytical Chemistry*, *409*(29), 6813–6819.
- Noda, T., Isono, N., Krivandin, A. V., Shatalova, O. V., Błaszczak, W., & Yuryev, V. P. (2009). Origin of defects in assembled supramolecular structures of sweet potato starches with different amylopectin chain-length distribution. *Carbohydrate Polymers*, *76*(3), 400–409.
- Norouziyan, D., Akbarzadeh, A., Scharer, J. M., & Moo Young, M. (2006). Fungal glucoamylases. *Biotechnology Advances*, *24*(1), 80–85.
- Pan, D. D., & Jane, J.-I. (2000). Internal structure of normal maize starch granules revealed by chemical surface gelatinization. *Biomacromolecules*, *1*(1), 126–132.
- Pérez, S., & Bertoft, E. (2010). The molecular structures of starch components and their contribution to the architecture of starch granules: A comprehensive review. *Starch Stärke*, *62*(8), 389–420.
- Regina, A., Bird, A., Topping, D., Bowden, S., Freeman, J., Barsby, T., ... Morell, M. (2006). High-amylose wheat generated by RNA interference improves indices of large-bowel health in rats. *Proceedings of the National Academy of Sciences*, *103*(10), 3546–3551.
- Ring, S. G., l'Anson, K., & Morris, V. J. (1985). Static and dynamic light scattering studies of amylose solutions. *Macromolecules*, *18*(2), 182–188.
- Roder, N., Gerard, C., Verel, A., Bogracheva, T. Y., Hedley, C. L., Ellis, P. R., et al. (2009). Factors affecting the action of α -amylase on wheat starch: Effects of water availability. An enzymic and structural study. *Food Chemistry*, *113*(2), 471–478.
- Roman, L., Sahagun, M., Gomez, M., & Martinez, M. M. (2019). Nutritional and physical characterization of sugar-snap cookies: Effect of banana starch in native and molten states. *Food & Function*, *10*(2), 616–624.
- Sevenou, O., Hill, S. E., Farhat, I. A., & Mitchell, J. R. (2002). Organisation of the external region of the starch granule as determined by infrared spectroscopy. *International Journal of Biological Macromolecules*, *31*(1), 79–85.
- Shaik, S. S., Obata, T., Hebelstrup, K. H., Schwahn, K., Fernie, A. R., Mateiu, R. V., et al. (2016). Starch granule re-structuring by starch branching enzyme and glucan water dikinase modulation affects caryopsis physiology and metabolism. *PLoS One*, *11*(2), Article e0149613.
- Shrestha, A. K., Blazek, J., Flanagan, B. M., Dhital, S., Larroque, O., Morell, M. K., et al. (2012). Molecular, mesoscopic and microscopic structure evolution during amylase digestion of maize starch granules. *Carbohydrate Polymers*, *90*(1), 23–33.
- Shrestha, A. K., Jaroslav, B., Flanagan, B. M., Sushil, D., Oscar, L., Morell, M. K., et al. (2012). Molecular, mesoscopic and microscopic structure evolution during amylase digestion of maize starch granules. *Carbohydrate Polymers*, *90*(1), 23–33.
- Song, Y., Li, X., & Zhong, Y. (2019a). Optimization of butter, xylitol, and high-amylose maize flour on developing a low-sugar cookie. *Food Science and Nutrition*, *7*(11), 3414–3424.
- Song, Y., Li, X., & Zhong, Y. (2019b). Optimization of butter, xylitol, and high-amylose maize flour on developing a low-sugar cookie. *Food Science and Nutrition*, *7*(11), 3414–3424.
- Syahariza, Z., Sar, S., Hasjim, J., Tizzotti, M. J., & Gilbert, R. G. (2013). The importance of amylose and amylopectin fine structures for starch digestibility in cooked rice grains. *Food Chemistry*, *136*(2), 742–749.
- Tan, L., Flanagan, B. M., Halley, P. J., Whittaker, A. K., & Gidley, M. J. (2007). A method for estimating the nature and relative proportions of amorphous, single, and double-helical components in starch granules by ^{13}C CP/MAS NMR. *Biomacromolecules*, *8*(3), 885–891.
- Teng, A., Witt, T., Wang, K., Li, M., & Hasjim, J. (2016). Molecular rearrangement of waxy and normal maize starch granules during in vitro digestion. *Carbohydrate Polymers*, *139*, 10–19.
- Tian, Y., Li, M., Liu, X., Jane, J.-I., Guo, B., & Dhital, S. (2021). Storage temperature and time affect the enzyme resistance starch and glycemic response of cooked noodles. *Food Chemistry*, *344*, Article 128702.
- Tian, Y., Liu, X., Kirkensgaard, J. J. K., Khakimov, B., Enemark-Rasmussen, K., Hebelstrup, K. H., ... Zhong, Y. (2023). Characterization of different high amylose starch granules. Part I: Multi-scale structures and relationships to thermal properties. *Food Hydrocolloids*, Article 109286.
- Tian, Y., Wang, Y., Liu, X., Herburger, K., Westh, P., Møller, M. S., ... Blennow, A. (2023). Interfacial enzyme kinetics reveals degradation mechanisms behind resistant starch. *Food Hydrocolloids*, *140*, Article 108621.
- Wang, Y., Tian, Y., Christensen, S. J., Blennow, A., Svensson, B., & Møller, M. S. (2023). An enzymatic approach to quantify branching on the surface of starch granules by interfacial catalysis. *Food Hydrocolloids*, Article 109162.
- Wang, Y., Tian, Y., Zhong, Y., Suleiman, M. A., Feller, G., Westh, P., ... Svensson, B. (2023). Improved hydrolysis of granular starches by a psychrophilic α -Amylase starch binding domain-fusion. *Journal of Agricultural and Food Chemistry*, *71*(23), 9040–9050.
- Warren, F. J., Butterworth, P. J., & Ellis, P. R. (2013). The surface structure of a complex substrate revealed by enzyme kinetics and Freundlich constants for α -amylase interaction with the surface of starch. *Biochimica et Biophysica Acta (BBA)-General Subjects*, *1830*(4), 3095–3101.
- Weurding, R. E., Enting, H., & Versteegen, M. W. A. (2003). The effect of site of starch digestion on performance of broiler chickens. *Animal Feed Science and Technology*, *110*(1–4), 175–184.
- Witt, T., Gidley, M. J., & Gilbert, R. G. (2010). Starch digestion mechanistic information from the time evolution of molecular size distributions. *Journal of Agricultural and Food Chemistry*, *58*(14), 8444.
- Wong, K., & Jane, J. (1995). Effects of pushing agents on the separation and detection of debranched amylopectin by high-performance anion-exchange chromatography with pulsed amperometric detection. *Journal of Liquid Chromatography & Related Technologies*, *18*(1), 63–80.
- Worsøe, J., Fynne, L., Gregersen, T., Schlageter, V., Christensen, L. A., Dahlerup, J. F., ... Krogh, K. (2011). Gastric transit and small intestinal transit time and motility assessed by a magnet tracking system. *BMC Gastroenterology*, *11*(1), 1–10.
- Yu, W., Li, H., Zou, W., Tao, K., Zhu, J., & Gilbert, R. G. (2019). Using starch molecular fine structure to understand biosynthesis-structure-property relations. *Trends in Food Science & Technology*, *86*, 530–536.
- Yu, W., Zou, W., Dhital, S., Wu, P., Gidley, M. J., Fox, G. P., et al. (2018). The adsorption of α -amylase on barley proteins affects the in vitro digestion of starch in barley flour. *Food Chemistry*, *241*, 493–501.
- Zhang, X., Feng, J., Wang, H., Zhu, J., Zhong, Y., Liu, L., ... Xue, J. (2018). Bivariate flow cytometric analysis and sorting of different types of maize starch grains. *Cytometry, Part A*, *93*(2), 213–221.
- Zhong, Y., Bertoft, E., Li, Z., Blennow, A., & Liu, X. (2020). Amylopectin starch granule lamellar structure as deduced from unit chain length data. *Food Hydrocolloids*, *108*, Article 106053.
- Zhong, Y., Liu, L., Qu, J., Blennow, A., Hansen, A. R., Wu, Y., ... Liu, X. (2020). Amylose content and specific fine structures affect lamellar structure and digestibility of maize starches. *Food Hydrocolloids*, *108*, Article 105994.
- Zhong, Y., Qu, J., Blennow, A., Liu, X., & Guo, D. (2021). Expression pattern of starch biosynthesis genes in relation to the starch molecular structure in high-amylose maize. *Journal of Agricultural and Food Chemistry*, *69*(9), 2805–2815.

Zhong, Y., Qu, J. Z., Liu, X., Ding, L., Liu, Y., Bertoft, E., ... Blennow, A. (2022). Different genetic strategies to generate high amylose starch mutants by engineering the starch biosynthetic pathways. *Carbohydrate Polymers*, 287, Article 119327.

Zhong, Y., Tai, L., Blennow, A., Ding, L., Herburger, K., Qu, J., et al. (2022). High-amylose starch: Structure, functionality and applications. *Critical Reviews in Food Science and Nutrition*, 1–23.

Zhong, Y., Wu, Y., Blennow, A., Li, C., Guo, D., & Liu, X. (2020). Structural characterization and functionality of starches from different high-amylose maize hybrids. *Lebensmittel-Wissenschaft & Technologie*, 134, Article 110176.